

# Fragmentation functions in SUSY QCD and UHECR spectra produced in top-down models

R. Aloisio<sup>1</sup>, V. Berezhinsky<sup>1</sup> and M. Kachelrieß<sup>2</sup>

<sup>1</sup>*INFN, Laboratori Nazionali del Gran Sasso, I-67010 Assergi (AQ), Italy*

<sup>2</sup>*Max-Planck-Institut für Physik (Werner-Heisenberg-Institut), D-80805 München*

November 11, 2018

## Abstract

We present results from two different methods for the calculation of hadron spectra in QCD and SUSY QCD with large primary energies  $\sqrt{s}$  up to  $10^{16}$  GeV. The two methods considered are a Monte Carlo (MC) simulation and the evolution of fragmentation functions described by the Dokshitzer-Gribov-Lipatov-Altarelli-Parisi (DGLAP) equations. We find that the pion, nucleon and all-hadron spectra calculated with the two methods agree well. The MC simulation is performed with new hadronization functions (in comparison with our previous work), motivated by low-energy ( $\sqrt{s} < M_Z$ ) data and DGLAP. The hadron spectra calculated with both sets of hadronization functions agree well, which indicates that our method for calculating the hadronization function works successfully. The small difference in the calculated hadron spectra characterizes the uncertainties of this method. We calculate also the spectra of photons, neutrinos and nucleons and compare them with other published results. The agreement is good for all  $x$  from  $\sim 10^{-5}$  up to  $x \leq 0.3$ . The consistency of the spectra calculated by different methods allows to consider the spectral shape as a signature of models with decays or annihilations of superheavy particles, such as topological defects or superheavy DM. The UHECR spectra from these sources are calculated.

Key words: Perturbative calculations in QCD, Supersymmetry, Cosmic rays

PACS numbers: 11.30.Pb, 12.38.Bx, 96.40.-z.

# 1 Introduction

Ultra-High Energy Cosmic Rays (UHECR) remain a puzzle in physics. First of all, eleven AGASA [1] events with  $E \geq 1 \times 10^{20}$  eV contradict the Greisen-Zatsepin-Kuzmin (GZK) cutoff [2], although the HiRes data [3] are generally considered to be consistent with the GZK cutoff [4]. If the UHECR primaries are protons (see below) and if they propagate rectilinearly, as the claimed correlations with BL Lacs at lower energies  $(4-8) \times 10^{19}$  eV [5] imply, then their sources must be seen in the direction of the highest energy events with  $E \sim (2-3) \times 10^{20}$  eV detected by HiRes [3], Fly's Eye [6] and AGASA [7]. Indeed, the proton attenuation length at these energies is only 20 – 30 Mpc [8], and the sources should have been seen in the direction of these particles, since such correlations exist at considerably lower energies. This implies that particles with  $E \sim 10^{20}$  eV may have a different origin as those with lower energies.

Meanwhile, there is strong evidence that primary particles at lower energies,  $1 \times 10^{18} \lesssim E \lesssim (7-8) \times 10^{19}$  eV, are extragalactic protons, most probably from Active Galactic Nuclei (AGN). The different pieces of evidence include: (*i*) Extensive Air Shower (EAS) data confirm protons as primaries [9, 10], (*ii*) the dip [11], seen with  $\chi^2_{\text{dof}} = 0.7$  in the spectra of AGASA, HiRes, Fly's Eye and Yakutsk [12], is a signature of the propagation of UHE protons in the extragalactic space and (*iii*) the beginning of the GZK cutoff seen in the spectra of AGASA and HiRes [12].

According to the correlations with BL Lacs found in Ref. [5] and the analysis of small-angle clustering [13], protons should propagate rectilinearly from the sources (AGN). However, if one excludes the correlations with BL Lacs from the analysis, the propagation of protons in very strong magnetic fields becomes also feasible [14, 15]. Nevertheless, also in this case, the lack of a nearby source in the direction of the highest energy events (e.g. at  $E \sim 3 \times 10^{20}$  eV) remains a problem for reasonable field strengths  $B \sim 1$  nG: the deflection angle,  $\theta \sim l_{\text{att}}/r_H = 3.7^\circ B_{\text{nG}}$  given by the attenuation length  $l_{\text{att}}$  and the Larmor radius  $r_H$ , is small and sources should be seen.

Many ideas have been put forward aiming to explain the observed superGZK ( $E \gtrsim (6-8) \times 10^{19}$  eV) events: strongly interacting neutrinos [16] and new light hadrons [17] as unabsorbed signal carriers,  $Z$ -bursts [18], Lorentz-invariance violation [19], Topological Defects (TD) (see [20] for a review), and Superheavy Dark Matter (SHDM) (see [21] for a review).

The two last models listed above share a common feature: UHE particles are produced in the decay of superheavy (SH) particles or in their annihilation. In the case of TD they are unstable and in the case of SHDM long-lived particles. We shall call them collectively  $X$  particles. In the  $Z$ -burst model, the decay of a much lighter particle, the  $Z$ -boson, is involved, while the decay products are boosted by very large Lorentz factors. Annihilation takes place in the case of monopolonia [22], necklaces [23] and SHDM particles within some special models [24]. As elementary particle physics is concerned, both processes proceed in a way similar to  $e^+e^-$  annihilation into hadrons: two or more off-mass-shell quarks and gluons are produced and they initiate QCD cascades. Finally the partons are hadronized at the confinement radius. Most of the hadrons in the final state are pions and thus the typical prediction of all these models is the dominance of photons at the highest energies  $E \gtrsim (6-8) \times 10^{19}$  eV.

This prediction is questioned by the AGASA data [25] at  $E \gtrsim 1 \times 10^{20}$  eV combined with the recent recalculation [26] of the muon number in photon-initiated EAS at the highest energies. Previously [27, 28], the muon content in photon-induced showers was found to be similar to that in proton-induced showers. According to the new calculations,

the muon number is still large, but 5 – 10 times smaller than in hadronic showers. From eleven AGASA events at  $E \gtrsim 1 \times 10^{20}$  eV, the muon content is measured in six and in two of them it is high. The muon content of the remaining four events is close to the one in photon-induced showers. MC simulations [25] show that a primary flux comprised *completely* by photons is disfavored. We shall discuss further these data in the Conclusions.

The spectrum of hadrons produced in the decay/annihilation of  $X$  particles is another signature of models with superheavy  $X$  particles. Several methods for the calculation of these spectra have been developed in the past several years.

The mass of the decaying particle,  $M_X$ , or the energy of annihilation  $\sqrt{s}$ , is in the range  $10^{13} - 10^{16}$  GeV. The existing QCD MC codes become numerically unstable at much smaller energies, e.g., at  $M_X \sim 10^7$  GeV in the case of HERWIG. Moreover, the computing time increases rapidly going to larger energies. Nevertheless, one of the first spectrum calculation has been performed with the help of HERWIG for energies up to  $M_X \sim 10^{11}$  GeV, and the computed spectra were extrapolated to  $M_X \sim 10^{13}$  GeV [29]. Supersymmetry was not included in these calculations.

Another option used in the first calculations is the *limiting spectrum*, an analytic method developed in Refs. [30]. This method has been found to be very successful at LEP energies (see [31] and references therein). Two basic assumptions are involved in this method: (i) the beta function  $\beta$  describing the running of the QCD coupling  $\alpha_s$  is taken to be constant, i.e.  $\alpha_s(k_\perp^2) \propto 1/\ln(k_\perp^2/\Lambda^2)$  for all transverse momenta  $k_\perp$ , and (ii) the minimum virtuality  $Q_0$  of partons, down to which the cascade develops perturbatively, is taken equal to the scale  $\Lambda$ . The high energy supersymmetric generalization of this solution has been obtained in Ref. [32]. Later, a comparison with the MC simulation [33] showed that the limiting spectrum does not describe well hadron spectra in SUSY QCD and that the assumption (i) is mainly responsible for the discrepancies found. Indeed, changing the evolution of  $\alpha_s(k_\perp^2)$  an agreement of the spectra around the Gaussian peaks was obtained [33] when in the SUSY QCD MC  $\alpha_s$  with  $\beta = \text{const.}$  was used and  $\alpha_s$  was frozen at small  $k_\perp^2$ , which is a reasonable physical assumption, e.g., in the DGLAP method<sup>1</sup>. For more details see Ref. [33].

Monte Carlo simulations are the most physical approach for high energy calculations which allow to incorporate many important physical features as the presence of SUSY partons in the cascade and coherent branching [35]. The perturbative part of our MC simulation is similar to other existing MC programs and hence reliable.

For the non-perturbative hadronization part a phenomenological approach is used in Ref. [33]. The fragmentation of parton  $i$  into a hadron  $h$  is expressed through perturbative fragmentation function of partons  $D_i^j(x, M_X)$  convoluted with hadronization functions  $f_j^h(x, Q_0)$  at the scale  $Q_0$ ,

$$D_i^h(x, M_X) = \sum_{j=q,g} \int_x^1 \frac{dz}{z} D_i^j(x/z, M_X, Q_0) f_j^h(z, Q_0), \quad (1)$$

where the hadronization functions do not depend on the scale  $M_X$  (as notation for the scale in this paper we shall use also  $\sqrt{s} = M_X$  and  $t = \ln(s/s_0)$ ). This important property of hadronization functions allows us to calculate  $f_i^h(x, Q_0)$  from available LEP data,  $D_i^h(x, M_X)$  at the scale  $M_X = M_Z$ , and then to use it for the calculation of fragmentation functions  $D_i^h(x, M_X)$  at any arbitrary scale  $M_X$ . Our approach reduces the computing time compared to usual MC simulations and allows the fast calculation of hadron spectra

---

<sup>1</sup>We are not able to find any place in our paper [33] where according to [34] we “acknowledge errors.”

for large  $M_X$  up to  $M_{\text{GUT}}$ . The MC of Ref. [33] has two versions: one for ordinary QCD and another one for SUSY QCD.

The perturbative part of the MC simulation in Ref. [33] includes standard features such as angular ordering, which provides the coherent branching and the correct Sudakov form factors, as well as SUSY partons. Taking into account SUSY partons results only in small corrections to the production of hadrons, and therefore a simplified spectrum of SUSY masses works with good accuracy.

The weak influence of supersymmetry is explained by the decay of SUSY partons, when the scale of the perturbative cascade reaches the SUSY scale  $Q_{\text{SUSY}}^2 \sim 1 \text{ TeV}^2$ . Most of the energy of SUSY partons remains in the cascade in the form of energy of ordinary partons, left after the decay of SUSY partons. The qualitatively new effect caused by supersymmetry is the effective production of the Lightest Supersymmetric Particles (LSP), which could be neutralinos or gluinos. The spectra of neutralinos were calculated in [33].

MC simulations allow also to calculate the characteristic feature of the QCD spectrum, the Gaussian peak, which is beyond the power of the next method we shall review.

The fragmentation functions  $D_i^h(x, M_X)$  at a high scale  $M_X$  can be calculated evolving them from a low scale, e.g.  $M_X = M_Z$ , where they are known experimentally. This evolution is described by the Dokshitzer-Gribov-Lipatov-Altarelli-Parisi (DGLAP) equation [36, 37] which can be written schematically as

$$\partial_t D_i^h = \sum_j \frac{\alpha_s(t)}{2\pi} P_{ij}(z) \otimes D_j^h(x/z, t), \quad (2)$$

where  $t = \ln(s/s_0)$ ,  $\otimes$  denotes the convolution  $f \otimes g = \int_z^1 dx/x f(x)g(x/z)$ , and  $P_{ij}$  is the splitting function which describes the emission of parton  $j$  by parton  $i$ . Apart from the experimentally rather well determined quark fragmentation function  $D_q^h(x, M_Z)$ , also the gluon FF  $D_g^h(x, M_Z)$  is needed for the evolution of Eq. (2). The gluon FF can be taken either from MC simulations or from fits to experimental data, in particular to the longitudinal polarized  $e^+e^-$  annihilation cross-section and three-jet events.

The first application of this method for the calculation of hadron spectra from decaying superheavy particles has been made in Refs. [38, 39], followed by Refs. [34, 40, 41, 42, 43, 44]. The most detailed calculations have been performed in Ref. [44], where more than 30 different particles were allowed to be cascading and the mass spectrum of the SUSY particles was taken into account. Although at  $M_Z$ , which is normally the initial scale in the DGLAP method, the fragmentation functions for supersymmetric partons are identically zero, they can be calculated at larger scales  $t$ : SUSY partons are produced above their mass threshold, when their splitting functions are included in Eq. (2). In this work we prove that this method is correct. Also, the LSP spectrum can be computed within the DGLAP approach [44, 45].

A problem of the DGLAP method are the fragmentation functions at small  $x = 2p/\sqrt{s}$ , where  $p$  is the momentum. The DGLAP equations allow to evolve fragmentation functions known at  $x > x_{\text{min}}$  from a starting scale  $\sqrt{s_0}$  to a higher scale  $\sqrt{s}$ . Therefore,  $x_{\text{min}}$  of the FF at the starting scale  $\sqrt{s_0}$  determines the  $x$  range accessible for *all*  $s$ . Requiring that perturbation theory can be used,  $p_{\perp} > \Lambda \sim 0.25 \text{ GeV}$ , leads for the starting scale  $M_Z$  to  $x > 0.005$ .

In Ref. [43, 44] the initial fragmentation functions are taken from Ref. [46] at the scale  $Q_0 \sim 1.4 \text{ GeV}$  and are extrapolated to very low  $x \sim 10^{-5}$ , i.e. into the non-perturbative region. The formal DGLAP evolution between the scales  $Q_0$  and  $M_Z$  is described by

equations with  $\alpha_s(s)$  not depending on  $x$  (see e.g. Eq. (10) in Section 2). Surprisingly enough this method works well: The fragmentation functions for  $x$  as low as  $10^{-5}$  evolved in Ref. [43, 44] to large  $M_X$  coincide with our MC simulation.

Near the GUT scale all three gauge couplings  $\alpha_i$  ( $i = 1, 2, 3$ ) have approximately equal numerical values. Naively one expects that at scales  $M_X$  close enough to the GUT scale all particles including e.g. leptons and electroweak (EW) gauge bosons are cascading like QCD partons.

In fact, the influence of the masses of the EW gauge bosons on soft singularities has to be carefully studied. In the MC approach, the leading effect of the finite masses of the gauge boson can be implemented in a rather straightforward way [47]. Cascading of the longitudinal modes of the EW gauge bosons or of the Higgs bosons is a subleading effect. In Ref. [47], it was demonstrated that EW cascading occurs at  $M_X \gtrsim 10^6$  GeV, even if only leptons and EW bosons are included in the consideration. The interactions with quarks and gluons mixes EW and QCD cascades. If, for example, a hypothetical  $X$  particle couples at tree level only to neutrinos, their further cascading results in the production of the QCD partons and thus of hadrons. Thus the production of neutrinos through decays of  $X$  particles with such couplings is constrained by the usual electromagnetic (e-m) cascade limit in the universe. EW cascading has been included in the calculations of Refs. [43, 44], though in a formal way.

In this paper we shall study the agreement of two methods: MC and DGLAP equations for the calculation of spectra produced in the decay or annihilation of superheavy particles. For this we shall calculate the spectra using the same assumptions in both methods. We shall also compare the results obtained by different groups and confront the calculated spectra with recent ones measured by UHECR experiments.

The paper is organized as follows: in Section 2 we introduce the DGLAP equations and the technique used to solve them. In Section 3 we discuss the properties of the hadronization functions used in the MC simulation and obtain new low-energy motivated hadronization functions as extension of those used in [33]. Then we compare the fragmentation functions calculated with the MC and the DGLAP equations in Section 4. Photon, neutrino and proton spectra, needed for UHECR calculations, are computed in Section 5 and compared with the spectra obtained in Refs. [34, 43, 44]. Finally, in Section 6 we consider the consequences of our results for models of superheavy DM and Topological Defects.

## 2 DGLAP equations in SUSY QCD

If the  $X$  particle decays into partons  $i = u, \bar{u}, \dots, g$ , the parton FFs  $D_i^h(x, m_X^2)$  can be defined as the probability of fragmentation of a parton  $i$  into a hadron  $h$  with momentum fraction  $x = 2p/M_X$ . The evolution of FFs with increasing scale  $s = M_X^2$  (or  $t = \ln s/s_0$ ) is governed by the DGLAP equations,

$$\partial_t D_j^h(x, t) = \sum_i \int_x^1 \frac{dz}{z} D_i^h(x/z, t) P_{i \rightarrow j}(z, t). \quad (3)$$

Multiplying Eq. (3) by  $x$  and integrating it over  $x$  shows that the DGLAP equations conserve momentum,  $\partial_t \int D_j^h(x, t) x dx = 0$ , if  $\sum_j \int P_{i \rightarrow j}(x) x dx = 0$ .

Since in the limit  $s \gg m_q^2$  all quark flavors couple to gluons in the same way, the gluon

FF mixes only with the flavor singlet FF of quarks,

$$D_q^h(x, t) = \frac{1}{n_f} \sum_{\text{flavors}} \left( D_{q_i}^h(x, t) + D_{\bar{q}_i}^h(x, t) \right), \quad (4)$$

where the summation goes over the number of active quark flavors  $n_f$  involved in the process ( $n_f$  increases with increasing scale  $t$ ).

The coupled evolution equation for the gluon FF  $D_g^h$  and the quark singlet FF  $D_q^h$  becomes then

$$\partial_t \begin{pmatrix} D_q^h(x, t) \\ D_g^h(x, t) \end{pmatrix} = \left[ \begin{pmatrix} P_{qq}(x, t) & P_{gq}(x, t) \\ 2n_f P_{qg}(x, t) & P_{gg}(x, t) \end{pmatrix} \otimes \begin{pmatrix} D_q^h(x, t) \\ D_g^h(x, t) \end{pmatrix} \right], \quad (5)$$

where  $\otimes$  denotes as usually the convolution  $[f \otimes g](z) \equiv \int_z^1 dx/x f(x)g(x/z) = \int_z^1 dx/x f(x/z)g(x)$ , and  $P_{ij} \equiv P_{i \rightarrow j}$ .

A formal extension of the standard DGLAP equations (5) to the SUSY case is straightforward. Denoting squark and gluino by  $\tilde{q}$  and  $\tilde{g}$ , respectively, and considering the flavor singlet FF for squarks as it was discussed for quarks, we can write the SUSY DGLAP equations as

$$\partial_t \begin{pmatrix} D_q^h(x, t) \\ D_{\tilde{q}}^h(x, t) \\ D_g^h(x, t) \\ D_{\tilde{g}}^h(x, t) \end{pmatrix} = \left[ \begin{pmatrix} P_{qq}(x, t) & P_{gq}(x, t) & P_{\tilde{q}q}(x, t) & P_{\tilde{g}q}(x, t) \\ 2n_f P_{qg}(x, t) & P_{gg}(x, t) & 2n_f P_{\tilde{q}g}(x, t) & P_{\tilde{g}g}(x, t) \\ P_{q\tilde{q}}(x, t) & P_{g\tilde{q}}(x, t) & P_{\tilde{q}\tilde{q}}(x, t) & P_{\tilde{g}\tilde{q}}(x, t) \\ 2n_f P_{q\tilde{g}}(x, t) & P_{g\tilde{g}}(x, t) & 2n_f P_{\tilde{q}\tilde{g}}(x, t) & P_{\tilde{g}\tilde{g}}(x, t) \end{pmatrix} \otimes \begin{pmatrix} D_q^h(x, t) \\ D_{\tilde{q}}^h(x, t) \\ D_g^h(x, t) \\ D_{\tilde{g}}^h(x, t) \end{pmatrix} \right]. \quad (6)$$

The exact form of the splitting functions  $P_{ij}(x, t)$  is not known, but using the perturbative expansion of these quantities one has

$$P_{ij}(x, t) = \sum_{n=0}^{\infty} \left( \frac{\alpha_s(t)}{2\pi} \right)^{n+1} P_{ij}^{(n)}(x) = \frac{\alpha_s(t)}{2\pi} P_{ij}^{(0)}(x) + \mathcal{O}(\alpha_s^2). \quad (7)$$

The LO splitting functions of SUSY QCD were derived in Ref. [48] and are given in their unregularized form  $\hat{P}_{ij}$  in Table 1.

In the case of the diagonal splitting functions, we have to distinguish between regularized splitting functions  $P_{ii}(x)$  and unregularized ones  $\hat{P}_{ii}(x)$ . These splitting functions have a probabilistic interpretation only for  $x < 1$ , since they contain a delta function contribution at  $x = 1$  accounting for losses. Moreover, they describe the emission of soft gluons for  $x \rightarrow 1$  and contain therefore a pole of infrared type which needs to be regularized. Using momentum conservation,

$$\int_0^1 dz z [P_{qq}^{(0)}(z) + P_{gq}^{(0)}(z) + P_{\tilde{q}q}^{(0)}(z) + P_{\tilde{g}q}^{(0)}(z)] = 1 \quad (8a)$$

$$\int_0^1 dz z [2n_f P_{qg}^{(0)}(z) + P_{gg}^{(0)}(z) + 2n_f P_{\tilde{q}g}^{(0)}(z) + P_{\tilde{g}g}^{(0)}(z)] = 1 \quad (8b)$$

$$\int_0^1 dz z [P_{q\tilde{q}}^{(0)}(z) + P_{g\tilde{q}}^{(0)}(z) + P_{\tilde{q}\tilde{q}}^{(0)}(z) + P_{\tilde{g}\tilde{q}}^{(0)}(z)] = 1 \quad (8c)$$

$$\int_0^1 dz z [2n_f P_{q\tilde{g}}^{(0)}(z) + P_{g\tilde{g}}^{(0)}(z) + 2n_f P_{\tilde{q}\tilde{g}}^{(0)}(z) + P_{\tilde{g}\tilde{g}}^{(0)}(z)] = 1, \quad (8d)$$

one obtains as formal expression for the regularized splitting functions

$$P_{qq}^{(0)}(x) = \hat{P}_{qq}^{(0)}(x) - \delta(1-x) \int_0^1 dz z [\hat{P}_{qq}^{(0)}(z) + P_{gq}^{(0)}(z) + P_{\tilde{q}q}^{(0)}(z) + P_{\tilde{g}q}^{(0)}(z)] \quad (9a)$$

$$P_{gg}^{(0)}(x) = \hat{P}_{gg}^{(0)}(x) - \delta(1-x) \int_0^1 dz z [2n_f \hat{P}_{qg}^{(0)}(z) + P_{gg}^{(0)}(z) + 2n_f P_{\bar{q}g}^{(0)}(z) + P_{g\bar{g}}^{(0)}(z)] \quad (9b)$$

$$P_{\bar{q}\bar{q}}^{(0)}(x) = \hat{P}_{\bar{q}\bar{q}}^{(0)}(x) - \delta(1-x) \int_0^1 dz z [\hat{P}_{\bar{q}\bar{q}}^{(0)}(z) + P_{g\bar{q}}^{(0)}(z) + P_{\bar{q}g}^{(0)}(z) + P_{\bar{g}\bar{g}}^{(0)}(z)] \quad (9c)$$

$$P_{\bar{g}\bar{g}}^{(0)}(x) = \hat{P}_{\bar{g}\bar{g}}^{(0)}(x) - \delta(1-x) \int_0^1 dz z [2n_f \hat{P}_{q\bar{g}}^{(0)}(z) + P_{g\bar{g}}^{(0)}(z) + 2n_f P_{\bar{q}\bar{g}}^{(0)}(z) + P_{\bar{g}\bar{g}}^{(0)}(z)]. \quad (9d)$$

Instead of calculating explicitly the expressions after the delta functions, we substitute Eqs. (9a–9d) directly into the DGLAP equations. In the case of ordinary QCD, the evolution of the singlet quark FF is then given by

$$\begin{aligned} \partial_t D_q^h(x, t) = & \frac{\alpha_s(t)}{2\pi} \int_0^1 dz \left\{ \hat{P}_{qq}^{(0)}(z) \left[ \frac{1}{z} D_q^h\left(\frac{x}{z}, t\right) \Theta(z-x) - z D_q^h(x, t) \right] - \right. \\ & \left. z P_{gq}^{(0)}(z) D_q^h(x, t) \right\} + \frac{\alpha_s(t)}{2\pi} \int_x^1 \frac{dz}{z} P_{gq}^{(0)}(z) D_g^h\left(\frac{x}{z}, t\right), \end{aligned} \quad (10)$$

where  $\Theta$  denotes the usual step function. Since the two terms in the square bracket cancel each other for  $z = 1$ , the pole of  $\hat{P}_{qq}^{(0)}(z)$  disappears. The same method can be used to replace the other diagonal splitting functions by their unregularized counter-parts.

Energy conservation is automatically ensured by Eqs. (9a–9d).

The DGLAP equations allow to evolve the FFs  $D_i^h(x)$  known at some scale  $s_0$  to higher scales  $s$ . Since we are interested in a comparison of this method with our MC simulation, we use for the initial scale  $s_0 = M_Z^2$ , i.e. the same as we have used in the MC to derive the hadronization function. Alternatively, we shall use for the initial scale of evolution also the very low value  $\sqrt{s_0} \sim 1$  GeV as it will be explained in Section 3.

In the case of the initial scale  $M_Z$  one has two initial FFs,  $D_q^h(x, M_Z)$  and  $D_g^h(x, M_Z)$ . The former is known experimentally and the latter is calculated using our MC simulation. We shall describe now shortly some technical aspects connected with the numerical solution of the DGLAP equations. Starting from an initial set of FFs at given  $t$  and  $x$ , all FFs are evolved simultaneously with a 4th order Runge-Kutta algorithm with fixed step-size. At each Runge-Kutta step, the rhs of the DGLAP equations is evaluated with a Gaussian quadrature algorithm. Since this algorithm requires the knowledge of the FFs at  $x$  values different from the initially chosen ones, a polynomial interpolation algorithm is used to calculate the FFs. To avoid the  $1/z$  singularities in the integrand, we evolve  $x D_i^h(x, t)$  instead of  $D_i^h(x, t)$ .

For the evolution of  $\alpha_s(s)$  as a function of  $s$  we use the same method as in our MC simulation [33]: we combine the thresholds of gluinos and all squarks in a single threshold at  $s = M_{\text{SUSY}}^2$ . The numerical value of  $M_{\text{SUSY}}$  is then fixed by requiring unification of coupling constants as in the minimal SUSY SU(5) model. This simplified treatment of the SUSY mass spectrum allows to compare the two methods using the same assumptions. Since moreover the results depend only weakly on  $M_{\text{SUSY}}$ , this simplification is physically reasonable.

We shall finish this section with a remark on the connection between the more often discussed space-like evolution of structure functions  $f$  and the time-like evolution of fragmentation functions  $D$  describing (SUSY) QCD cascades [49]. Since  $D_j$  represents the fragmentation of the final parton  $j$ , while  $f_i$  describes the distribution of the initial parton  $i$ , the matrix of splitting functions  $P$  has to be transposed going from one case to the other, as

$$(P_{i \leftarrow j})_{ij, \text{space-like}} \leftrightarrow (P_{j \rightarrow i})_{ji, \text{time-like}}. \quad (11)$$

On the other hand, a formal analytic continuation relates the splitting functions in both regions at leading order (LO): neglecting color factors, this relation is

$$\left| [xP_{i \leftarrow j}(1/x)]_{\text{space-like}} \right| = \left| [P_{i \rightarrow j}(x)]_{\text{time-like}} \right|. \quad (12)$$

Performing both transformations, the DGLAP equations are identical in the time- and space-like region at LO.

Since in Refs. [34, 45] only the transformation (11) has been performed, the splitting functions there (most notably for gluons and gluinos) are different from ours and from those in Refs. [43, 44], where both transformations (11) and (12) have been correctly used.

### 3 Hadronization functions in the Monte Carlo simulation

In this Section we discuss the general properties of the hadronization functions used in the MC simulation and their connection with the DGLAP method.

In the MC simulation the hadronization functions are defined by Eq. (1). They can be determined from the FFs at lower scales, e.g at  $M_X = M_Z$ , known from  $e^+e^- \rightarrow$  hadrons data. Namely, we take the measured all-hadron spectrum as FF  $D_q^h(x, M_Z)$  as lhs of Eq. (1) and compute the hadronization functions at the rhs of this equation.

However, hadronization functions cannot be calculated in an unique way using Eq. (1): Only if the FF function  $D_q^h(x, M_Z)$  were known precisely at an infinite number of points  $x$ , then the hadronization functions  $f_j(x)$  could be calculated in principle in an unique way using e.g. the method of inversion. In practice the number of points  $x$ , where the FFs are measured is limited, and the experimental errors at some of them (most notably at  $x$  close to 1) are large. Another uncertainty arises if the flavor dependence of FFs is considered. The arbitrary choice of the minimal virtuality  $Q_0$  of partons in the MC also introduces some additional error: Although the rhs of Eq. (1) should not depend on  $Q_0$ , in practice all MC simulations yield slightly different results for different  $Q_0$ .

Instead of using the inversion method, we assume a specific functional form of the hadronization function, characterized by a set of free parameters, and perform then a fit to the data. In this method additional uncertainties appear, because the functional form has to be specified a priori. As a result one can obtain different hadronization functions within the uncertainties discussed above. Deriving a new set of hadronization functions in this paper, we estimate as by-product the corresponding uncertainties in the calculated spectra.

In Ref. [33] we have used two hadronization functions—one for the quark flavor singlet and another for the gluons—motivated by the limiting spectrum. Each of them contains three free parameters and we have determined these parameters using the observed spectrum of charged hadrons at  $\sqrt{s} = M_Z$ . Then we performed several tests to check our hadronization scheme (see Ref. [33]). Among them are the calculation of hadron spectra at two other scales,  $\sqrt{s} = 58$  GeV and  $\sqrt{s} = 133$  GeV, where measurements are available. We also mention here one particular test based on the limiting spectrum. We run our ordinary QCD MC with the hadronization functions fixed as above using the same set of assumptions which are used in the derivation of the limiting spectrum: we fixed the number of flavors to  $n_f = 3$  (or to  $n_f = 6$ ) and the running of  $\alpha_s$  was taken exactly as in



the limiting spectrum method. We obtained an excellent agreement at all scales  $M_X$  and for all  $x$  except those close to one, where the limiting spectrum is invalid.

The FFs in these calculations,  $D_i^h(x, M_X)$  and  $D_i^j(x, M_X)$ , conserve momentum exactly and with good accuracy, respectively.

In this Section we shall use another choice of hadronization functions, imposing low-energy data and some additional physical interpretation motivated by the DGLAP equations, and demonstrate that the calculated spectra for different  $M_X$  agree well with our previous calculations.

We shall begin with the general properties of fragmentation and hadronization functions, which we impose on those used in our calculations.

(i) *Momentum conservation of hadrons,*

$\sum_h \int_0^1 D_i^h(x, s) x dx = 1$ , and partons  $\sum_j \int_0^1 D_i^j(x, s) x dx = 1$ , results in the normalization of the hadronization function as  $\sum_h \int_0^1 f_i^h(x) x dx = 1$ .

The proof follows from Eq. (1). Indeed,

$$1 = \sum_h \int_0^1 D_i^h(x, s) x dx = \sum_h \sum_j \int_0^1 x dx \int_x^1 \frac{dz}{z} D_i^j\left(\frac{x}{z}, s\right) f_j^h(z). \quad (13)$$

Changing the order of integration, using the variable  $x' = x/z$  and introducing the new function

$$\zeta_i^j(s) \equiv \int_0^1 D_i^j(x', s) x' dx', \quad (14)$$

one obtains

$$1 = \sum_h \sum_j \int_0^1 dz z f_j^h(z) \zeta_i^j(s), \quad (15)$$

which must hold for arbitrary  $s$ . Consistency with the condition  $\sum_j \zeta_i^j(s) = 1$  leads to

$$\sum_h \int_0^1 dz z f_i^h(z) = 1 \quad (16)$$

as the only solution.

Similarly, one can prove the reversed statement:

(ii) *The momentum conservation of partons in the perturbatively calculated cascade*  $\sum_j \int_0^1 D_i^j(x, s) x dx = 1$ , with the hadronization function normalized as in Eq.(16) results in momentum conservation of hadrons.

Now we add an assumption about hadronization functions which links MC and DGLAP methods, namely we assume that the hadronization function is a FF function  $D_i^h(x, \sqrt{s})$  extrapolated to the very low scale  $\sqrt{s} = Q_0$ . Then the FF  $D_i^h(x, \sqrt{s})$  can be computed with the help of DGLAP evolution equations using the hadronization function  $f_i^h(x, Q_0)$  as the initial FF. Under this assumption we should choose the hadronization function as the fragmentation function obtained for low energy  $e^+e^-$  annihilation and/or  $ep$  scattering. Namely, we take it following Ref. [50] as

$$f_i^h(x, Q_0) = N_i x^{a_i} (x + x_i)^{-b_i} (1 - x)^{c_i}, \quad (17)$$

where the index  $i$  runs through quark singlet  $q$  and gluon  $g$ , and the index  $h$  refers to the total hadron spectra. We fix the value of  $Q_0$  in our MC simulation as in Ref. [33] to  $Q_0^2 = 0.625 \text{ GeV}^2$ . As in [33], the parameters are found performing a  $\chi^2$  fit of the LEP spectrum at  $\sqrt{s} = M_Z$  by  $D_i^h(x, M_Z)$  calculated from Eq. (1). The hadronization

functions are shown in Fig. 1. Their main features agree with those of [33]:  $f_g$  has its maximum at  $x \sim 0.1$ , while  $f_q$  peaks close to  $x = 1$ . As a difference one can see that the new fit function is chosen to ensure  $f_q(x = 1) = 0$ .

In Figs. 2, 3 and 4, the spectra of hadrons  $D_q^h(x, \sqrt{s})$  calculated for the scales  $\sqrt{s} = 58$  GeV, 91.2 GeV, and 133 GeV are compared with observations. (The measurements are for charged hadrons and rescaled by us to the total hadron spectra.) In Figs. 5 and 6 these spectra computed at the scales  $\sqrt{s} = 1 \times 10^{10}$  GeV and  $1 \times 10^{16}$  GeV using the old [33] and new hadronization functions are shown. The agreement is good, as it has been expected. The ratio between the new and old spectra, shown in Fig. 7, illustrates the uncertainties in our MC simulations connected with different choices of hadronization functions. Figures 5, 6 and 7 show that these uncertainties affect only the high energy part of the spectrum at  $x > 0.1$ .

We described above the all-hadron spectra  $D_i^h(x, M_X)$ . Similar calculations have been performed by us for charged pions and nucleons, using the experimental data at  $\sqrt{s} = M_Z$  from the ALEPH and OPAL collaborations [53].

As a test of the interpretation of the MC hadronization function  $f_i^h(x, Q_0)$  as low energy limit of the FF  $D_i^h(x, \sqrt{s})$ , we have evolved the hadronization function given by Eq. (17) from the scale  $Q_0^2 = 0.625$  GeV<sup>2</sup> to the higher scales using our QCD DGLAP code described in Section 2. In principle, this procedure should not work well for very small  $x = 2p/Q_0$ , where one is physically in the non-perturbative regime (see Introduction). But using the DGLAP equations which prescribe  $s$  as argument of  $\alpha_s$ , we can perform formally the evolution calculations, as it was done in Refs. [46, 50] and [43, 44].

In Fig. 8 and 9 the evolved hadronization functions at the scale  $M_Z$  are compared with FFs  $D_i^h(x, M_Z)$  calculated with the MC. We find good agreement for  $D_g^h$  but much worse agreement for  $D_q^h$ . We think that a reason for this failure is the use of the quark flavor singlet FF at low scales. Indeed, in the successful evolution of the Refs. [43, 44, 46, 50], the FFs for different quarks have different parameterizations. For scales above  $M_Z$ , the flavor singlet FF becomes a good approximation, and, indeed, the evolution of hadronization functions from the scale  $Q_0$  to scale  $M_{\text{GUT}}$  results in very good agreement with MC simulation (see Fig. 10). In this case, the agreement is equally good for both  $D_q^h$  and  $D_g^h$ .

## 4 Comparison of DGLAP and MC hadron spectra

In this Section we shall compare the hadron spectra computed by the two methods discussed above, MC and DGLAP.

We shall begin with a remark concerning the smallest and largest  $x$  values of practical interest. Coherent branching produces the so-called Gaussian peak in multiplicity with maximum at  $x_{\text{max}} \sim (Q_0/M_X)^{0.6} \sim 2 \times 10^{-10}$  for  $M_X \sim M_{\text{GUT}}$ . This approximate estimate coincides well with the value found in the MC simulation [33]. Note that the DGLAP method is not valid for those  $x$  values where coherence plays an essential role, namely at  $x \lesssim 4 \times 10^{-5}$  (see Fig. 8 in Ref. [33]). The lowest value  $x_{\text{min}}$  relevant for physical applications is much higher than  $x_{\text{max}}$ :  $x_{\text{min}} \sim 2E_{\text{obs}}/M_X \sim 2 \times 10^{-6}$  for the same  $M_X \sim M_{\text{GUT}}$  and for  $E_{\text{obs}} > 1 \times 10^{10}$  GeV. On the other side, the maximal observed energy  $\sim 3 \times 10^{20}$  eV and the minimal  $M_X$  of interest,  $M_X \gtrsim 10^{12}$  GeV, restrict  $x$  to values much smaller than 0.6. Thus the value  $x = 0.6$  can be considered as the largest  $x$  of interest for existing experimental data.

In Fig. 11 we present a comparison of  $D_i^h(x, M_X)$  with  $i = q$  and  $M_X = 1 \times 10^{16}$  GeV calculated for ordinary QCD with the MC and DGLAP method. The initial scale in the DGLAP method is taken as  $\sqrt{s} = M_Z$ , but the initial scale  $\sqrt{s} = Q_0$  gives practically an identical spectrum. The spectra for  $i = g$  agree equally well, as well as the spectra for other high scales  $M_X$ .

One can see that the MC and DGLAP spectra slightly differ at very low  $x$  and have a more pronounced disagreement at large values of  $x$ . The discrepancy at low  $x$  is due to coherent branching, and it starts at the value of  $x$  estimated above ( $x \lesssim 4 \times 10^{-5}$ ). At large  $x$ , the calculations by both methods suffer from uncertainties, particularly the MC simulation. In this region the results are sensitive to the details of the hadronization scheme (see, e.g., the problem of HERWIG [38] with the overproduction of protons at large  $x$  and the dependence on the choice of the hadronization functions in our MC as illustrated by Figs. 5 and 6). One can add to this problem large uncertainties in the measured FFs at  $M_Z$  and  $x \sim 1$  and also the theoretical uncertainties connected with the models of  $X$  particle decay (unknown number and types of the initial partons<sup>2</sup> and unknown matrix element of the  $X$  particle decay).

However, as a whole, Fig. 11 demonstrates good agreement between MC and DGLAP methods. In Fig. 13 we present the ratio of FFs calculated with MC and DGLAP for ordinary QCD. At  $x \leq 1 \times 10^{-5}$  the MC FF is noticeably smaller than the DGLAP FF because coherence effects suppress branchings, an effect not included in the DGLAP method. At large  $x \geq 0.1$ , the discrepancy becomes greater than 20% due to the reasons explained above. For  $2.5 \times 10^{-5} \leq x \leq 0.1$ , the agreement between these two FFs is better than 20%.

Let us now come over to SUSY QCD.

In Fig. 12 we plot the FFs  $D_i^h(x, M_X)$  calculated by MC and DGLAP methods for  $M_X = 1 \times 10^{16}$  GeV and  $i = q$ . In the DGLAP method the SUSY FFs have been evolved from the ones obtained with the SUSY MC at the scale  $\sqrt{s} = 10M_{\text{SUSY}} \approx 10$  TeV. One can see the good agreement between DGLAP (solid curve) and MC (dotted curve). This good agreement holds also for other (lower) scales  $M_X$  and for other initial partons  $i = g, \tilde{g}, \tilde{q}$ . The ratio of FFs for SUSY MC and SUSY DGLAP is shown in Fig. 13.

When one does not have the initial SUSY FFs from a MC simulation, the question arises how to proceed. As was first suggested in Ref. [38, 40], the initial FFs can be taken as the ones for ordinary QCD at the low scale  $\sqrt{s} = M_Z$ , while the production of SUSY partons is included in the splitting functions assuming threshold behavior at  $M_{\text{SUSY}} \sim 1$  TeV. We can check this assumption computing the SUSY FF in both ways. In Fig. 12 we present the SUSY FFs  $D_i^h(x, M_X)$  for  $i = q$  and  $M_X = 1 \times 10^{16}$  GeV, evolved from the initial scale  $\sqrt{s} = M_Z$  (dashed curve). The good agreement between the two DGLAP curves proves the validity of the assumption made above.

## 5 Photon, neutrino and nucleon spectra

The spectra of photons, neutrinos and nucleons produced by the decay of superheavy particles are of practical interest in high energy astrophysics. These spectra  $D_i^a(x, M_X)$

---

<sup>2</sup> $X$  particles decay in many models due to nonperturbative interactions, and the number of primary partons is therefore model dependent. Since at large  $x$  the number of cascade generations is small, the FFs are for  $x \rightarrow 1$  rather sensitive to the initial multiplicity. In contrast, at small  $x$  when the number of cascade generations is large, differences in the initial multiplicity become inessential.

with  $a = \gamma, \nu, N$  can be also considered as FFs. Because the dependence on the type  $i$  of the primary parton is weak, we shall omit the index  $i$  from now on, keeping  $a$  as subscript.

Till now we concentrated our discussion on the total number of hadrons ( $a = h$ ) described by the FF  $D_h(x, M_X)$ , but in fact we have performed similar calculations separately for charged pions and protons+antiprotons. The procedure of the calculations is identical to that described in Section 2 for the DGLAP method and in Section 3 for the MC. For charged pions and protons+antiprotons we used experimental data from Refs. [53]. Below we shall present results of our SUSY MC simulations in terms of FFs for all pions  $D_\pi$ , all nucleons  $D_N$  and all hadrons  $D_h$ . We introduce the ratios  $\varepsilon_N(x)$  and  $\varepsilon_\pi(x)$  as

$$D_N(x) = \varepsilon_N(x)D_h(x), \quad D_\pi(x) = \varepsilon_\pi(x)D_h(x). \quad (18)$$

The spectra of pions and nucleons at large  $M_X$  have approximately the same shape as the hadron spectra, and one can use in this case  $\varepsilon_\pi = 0.73 \pm 0.03$  and  $\varepsilon_N = 0.12 \pm 0.02$ , taking into account the errors in the experimental data [51, 52, 53]. In Fig. 14 the ratios  $\varepsilon_N(x)$  and  $\varepsilon_\pi(x)$  are plotted as functions of  $x$  for different values of  $M_X$ . Note the peculiar dependence of  $\varepsilon_N(x)$  for small  $M_X$ . The smallness of  $\varepsilon_N(x)$  at small  $x$  and small  $M_X$  is caused formally by the smallness of the observed  $\pi/p$  ratio at  $M_X = M_Z$ , where we fit our FFs. Physically it is due to the combined effect of coherence and the mass difference of nucleons and pions. Indeed, the  $x$  values at small  $M_X$  where  $\varepsilon_N(x)$  is particularly small belong to the region below the Gaussian peak ( $x_m \sim (\Lambda/M_X)^{0.6}$ ), where coherence effects suppress branchings particularly strong.

We can calculate now the spectra of photons and neutrinos produced by the decays of pions neglecting the small contribution ( $0.15 \pm 0.04$ ) of  $K, D, \Lambda$  and other particles. Including these particles affects stronger neutrinos than photons, which are the main topic of this Section. For the pion spectrum we shall use  $D_\pi(x) = \varepsilon_\pi(x)D_h(x)$ .

The normalized photon spectrum from the decay of one  $X$  particle at rest is given by

$$D_\gamma(x) = \frac{2}{3} \int_x^1 \frac{dy}{y} \varepsilon_\pi(y) D_h(y). \quad (19)$$

The total neutrino spectrum from decays of charged pions and muons can be represented as [54]

$$D_\nu(x) = D_{\nu_\mu}^{\pi \rightarrow \mu \nu \mu}(x) + D_{\nu_\mu}^{\mu \rightarrow \nu \mu \nu e}(x) + D_{\nu_e}^{\mu \rightarrow \nu \mu \nu e}(x), \quad (20)$$

where for pion decay

$$D_{\nu_\mu}^{\pi \rightarrow \mu \nu \mu}(x) = \frac{2}{3} R \int_{xR}^1 \frac{dy}{y} \varepsilon_\pi(y) D_h(y) \quad (21)$$

with

$$R = (1 - m_\mu^2/m_\pi^2)^{-1}, \quad (22)$$

and for muon decay

$$D_{\nu_i}^{\mu \rightarrow \nu \mu \nu e}(x) = \frac{2}{3} \varepsilon_\pi R \int_x^1 \frac{dy}{y} q_i(y) \int_{x/y}^{x/ry} \frac{dz}{z} \varepsilon_\pi(z) D_h(z) \quad (23)$$

with

$$q_i = \frac{5}{3} - 3y^2 + \frac{4}{3}y^3 \text{ for } \nu_\mu, \bar{\nu}_\mu \quad \text{and} \quad q_i = 2(1 - 3y^2 + 2y^3) \text{ for } \nu_e, \bar{\nu}_e. \quad (24)$$

The spectra are presented in Fig. 15 for different masses  $M_X$ . We shall compare our photon spectra with those calculated by the DGLAP method in Refs. [43, 44] and

[34]. The photon spectrum is most interesting to compare, because it is straightforwardly related to the hadron spectrum which is the basic physical quantity. Moreover, the photon spectrum is the dominant component of radiation produced by superheavy particles.

To be precise, we compare the FF  $D_q^\gamma(x, M_X)$  at  $M_X = 1 \times 10^{16}$  GeV. Figure 16 demonstrates good agreement between our spectrum and those from Refs. [43, 44] at  $x \leq 0.3$ . As was it mentioned above, the disagreement at large  $x$  is not surprising. Apart from  $D_q^h(x, M_Z)$  taken directly from the experiments, both calculations use the much more uncertain  $D_g^h(x, Q^2)$ . In our case,  $D_g^h(x, Q^2)$  is taken from our MC simulation [33], in the case of Ref. [43, 44] from the fit performed in Ref. [46]. In both cases, rather large uncertainties exist at large  $x$  (e.g. see Fig. 5 from Ref. [46]). In both calculations the decay of the  $X$  particle into two partons is considered, but in fact in many models only many-parton decays exist. This and the unknown type of the initial partons add a common theoretical uncertainty to both calculations (see Section 4 for discussion)

The photon spectrum of Ref. [34] shows some deviation at  $x < 0.3$  from both spectra discussed above. To find the reason we performed the same calculations using splitting functions according the prescription of [34] (see Section 2) and obtained indeed some excess at small  $x$  and good agreement at large  $x$ , as one observes in Fig. 16. Nevertheless, the agreement between the three curves as presented in Fig. 16 is good.

In Fig. 17 we present also the comparison of our proton spectrum, computed with the SUSY QCD MC, with that of Refs. [43, 44] and [34], which shows good agreement.

## 6 UHECR from Superheavy DM and Topological Defects

As follows from Section 5, the accuracy of spectrum calculations has reached such a level that one can consider the spectral shape as a signature of the model. The predicted spectrum is approximately  $\propto dE/E^{1.9}$  in the region of  $x$  at interest, and it is considerably steeper than the QCD MLLA spectrum used in the end of 90s. The generation spectra for nucleons, neutrinos and gammas are shown Fig. 15.

Another interesting feature of these new calculations is a decrease of the ratio of photons to nucleons,  $\gamma/N$ , in the generation spectrum. This ratio is presented in Fig. 18 for  $M_X = 1 \times 10^{14}$  GeV by a solid curve together with a band of uncertainties given by the two dashed curves. At  $x \sim 1 \times 10^{-3}$  this ratio is characterized by a value of 2 – 3 only. The decrease of the  $\gamma/N$  ratio is caused by a decrease of the number of pions in the new calculations and by an increase of the number of nucleons. This result has an important impact for SHDM and topological defect models because the fraction of nucleons in the primary radiation increases. However, in both models photons dominate (i.e. their fraction becomes  $\gtrsim 50\%$ ) at  $E \gtrsim (7 - 8) \times 10^{19}$  eV (see below).

In this Section we shall consider two applications: superheavy dark matter (SHDM) and topological defects (TD).

UHECRs from SHDMs have been suggested in Refs. [55, 56] and further studied in Ref. [29]. Production of SHDM particles naturally occurs in the time-varying gravitational field of the expanding universe at the post-inflationary stage [57].

The relic density of these particles is mainly determined (at fixed reheating temperature and inflaton mass) by their mass  $M_X$ . The range of practical interest is  $(3 - 10) \times 10^{13}$  GeV, at larger masses the SHDM is a subdominant component of the DM.

SHDM is accumulated in the Galactic halo with the overdensity

$$\delta = \frac{\bar{\rho}_X^{\text{halo}}}{\rho_X^{\text{extr}}} = \frac{\bar{\rho}_{\text{DM}}^{\text{halo}}}{\Omega_{\text{CDM}}\rho_{\text{cr}}}, \quad (25)$$

where  $\bar{\rho}_{\text{DM}}^{\text{halo}} \approx 0.3 \text{ GeV/cm}^3$ ,  $\rho_{\text{cr}} = 1.88 \times 10^{-29} h^2 \text{ g/cm}^3$  and  $\Omega_{\text{CDM}} h^2 = 0.135$  [58]. With these numbers,  $\delta \approx 2.1 \times 10^5$ . Because of this large overdensity, UHECRs from SHDM have no GZK cutoff [55].

Clumpiness of SHDM in the halo can provide the observed small-angle clustering [59].

The quotient  $r_X = \Omega_X(t_0/\tau_X)$  of relic abundance  $\Omega_X$  and lifetime  $\tau_X$  of the  $X$  particle is fixed by the observed UHECR flux as  $r_X \sim 10^{-11}$ . The numerical value of  $r_X$  is theoretically calculable as soon as a specific particle physics and cosmological model is fixed. In the most interesting case of gravitational production of  $X$  particles, their present abundance is determined by their mass  $M_X$  and the reheating temperature  $T_R$ . The life-time of the  $X$  particles is on the other hand fixed by choosing a specific particle physics model. As shown in Ref. [60], there exist many models in which SH particles can be quasi-stable with lifetime  $\tau_X \gg 10^{10} \text{ yr}$ . The measurement of the UHECR flux, and thereby of  $r_X$ , selects from the three-dimensional parameter space  $(M_X, T_R, \tau_X)$  a two-dimensional subspace compatible with the SHDM hypothesis. *Such a determination of a priori free parameters from experimental data has nothing to do with fine-tuning*<sup>3</sup>, a reproach sometimes used against SHDM: Choosing a single value of  $\tau_X$  from the wide range of theoretically allowed values just reflects the present state of theoretical ignorance.

In Fig. 19, the spectra of UHE photons, neutrinos and protons from the decays of SHDM particles with  $M_X = 1 \times 10^{14} \text{ GeV}$  in the Galactic halo are presented. We have performed also a fit to the AGASA data using the photon flux from the SHDM model and the proton flux from uniformly distributed astrophysical sources. For the latter we have used the non-evolutionary model of Ref. [70]. The photon flux is normalized to provide the best fit to the AGASA data at  $E \geq 4 \times 10^{19} \text{ eV}$ . The fits are shown in Fig. 20 with  $\chi^2/\text{d.o.f.}$  indicated there.

*One can see from the fits in Fig. 20, that the SHDM model with the new spectra can explain only the excess of AGASA events at  $E \gtrsim 1 \times 10^{20} \text{ eV}$ : depending on the SHDM spectrum normalization and the details of the calculations for the extragalactic protons, the flux from SHDM decays becomes dominant only above  $(6 - 8) \times 10^{19} \text{ eV}$ .*

*Topological Defects* (for a review see [63]) can naturally produce UHE particles. The pioneering observation of this possibility has been made in Ref. [64].

The following TD have been discussed as potential sources of UHE particles: superconducting strings, ordinary strings, monopolonium (bound monopole-antimonopole pair), monopolonia (monopole-antimonopole pairs connected by a string), networks of monopoles connected by strings, vortons and necklaces (see Ref. [20] for a review and references).

Monopolonia and vortons are clustering in the Galactic halo and their observational signatures for UHECR are identical to SHDM. However, as has been demonstrated in Ref. [65], the friction of monopolonia in cosmic plasma results in monopolonium lifetime much shorter than the age of the universe.

Of all other TD which are not clustering in the Galactic halo, the most favorable for UHECR are *necklaces*. Their main phenomenological advantage is a small separation which ensures the arrival of highest energy particles to our Galaxy.

---

<sup>3</sup>In elementary-particle physics, fine-tuning is understood as tuning a quantity  $B$  to another quantity  $A$  with such precision that the predicted value  $m = A - B$  is many orders of magnitude smaller than  $A$  and  $B$ .

We shall calculate here the flux of UHECR from necklaces following the works [23, 62].

Necklaces are hybrid TD produced in the symmetry breaking pattern  $G \rightarrow H \times U(1) \rightarrow H \times Z_2$ . At the first symmetry breaking monopoles are produced, at the second one each (anti-) monopole get attached to two strings. This system resembles ordinary cosmic strings with monopoles playing the role of beads. Necklaces exist as the long strings and loops.

The symmetry breaking scales of the two phase transitions,  $\eta_m$  and  $\eta_s$ , are the main parameters of the necklaces. They determine the monopole mass,  $m \sim 4\pi\eta_m/e$ , and the mass of the string per unit length  $\mu \sim 2\pi\eta_s^2$ . The evolution of necklaces is governed by the ratio  $r \sim m/\mu d$ , where  $d$  is the average separation of a monopole and antimonopole along the string. As it is argued in Ref. [23], necklaces evolve towards configuration with  $r \gg 1$ . Monopoles and antimonopoles trapped in the necklaces inevitably annihilate in the end, producing heavy Higgs and gauge bosons ( $X$  particles) and then hadrons. The rate of  $X$  particles production in the universe can be estimated as [23]

$$\dot{n}_X \sim \frac{r^2\mu}{t^3 M_X}, \quad (26)$$

where  $t$  is the cosmological time.

The photons and electrons from pion decays initiate e-m cascades and the cascade energy density can be calculated as

$$\omega_{\text{cas}} = \frac{1}{2} f_\pi r^2 \mu \int_0^{t_0} \frac{dt}{t^3} \frac{1}{(1+z)^4} = \frac{3}{4} f_\pi r^2 \frac{\mu}{t_0^2}, \quad (27)$$

where  $z$  is the redshift and  $f_\pi \sim 1$  is the fraction of the total energy release transferred to the cascade.

The parameters of the necklace model for UHECR are restricted by the EGRET observations [66] of the diffuse gamma-ray flux. This flux is produced by UHE energy electrons and photons from necklaces due to e-m cascades initiated in collisions with CMB photons. In the range of the EGRET observations,  $10^2 - 10^5$  MeV, the predicted spectrum is  $\propto E^{-\alpha}$  with  $\alpha = 2$  [67]. The EGRET observations determined the spectral index as  $\alpha = 2.10 \pm 0.03$  and the energy density of radiation as  $\omega_{\text{obs}} \approx 4 \times 10^{-6}$  eV/cm<sup>3</sup>. The cascade limit consists in the bound  $\omega_{\text{cas}} \leq \omega_{\text{obs}}$ .

According to the recent calculations of Ref. [68], the Galactic contribution of gamma rays to the EGRET observations is larger than estimated earlier, and the extragalactic gamma-ray spectrum is not described by a power-law with  $\alpha = 2.1$ . In this case, the limit on the cascade radiation with  $\alpha = 2$  is more restrictive and is given by

$$\omega_{\text{cas}} \leq 2 \times 10^{-6} \text{ eV/cm}^3. \quad (28)$$

We shall use this limit in further estimates. Using Eq. (27) with  $f_\pi = 1$  and  $t_0 = 13.7$  Gyr [58] we obtain from Eq. (28)  $r^2\mu \leq 8.9 \times 10^{27}$  GeV<sup>2</sup>.

The important and unique feature of this TD is the small separation  $D$  between necklaces. It is given by  $D \sim r^{-1/2} t_0$  [23]. Since  $r^2\mu$  is limited by e-m cascade radiation, Eq. (27), we can obtain a lower limit on the separation between necklaces as

$$D \sim \left( \frac{3f_\pi\mu}{4t_0^2\omega_{\text{cas}}} \right)^{1/4} t_0 > 10(\mu/10^6 \text{ GeV}^2)^{1/4} \text{ kpc}. \quad (29)$$

This small distance is an unique property of necklaces allowing the unabsorbed arrival of particles with the highest energies.

The fluxes of UHECR from necklaces are shown in Fig.21 (the details of these calculations will be published in a forthcoming paper with P. Blasi [69]). We used in the calculations  $r^2\mu = 4.7 \times 10^{27} \text{ GeV}^2$  which corresponds to  $\omega_{\text{cas}} = 1.1 \times 10^{-6} \text{ eV/cm}^3$ , i.e. twice less than allowed by the bound (28). The mass of the  $X$  particles produced by monopole-antimonopole annihilations is taken as  $M_X = 1 \times 10^{14} \text{ GeV}$ .

From Fig. 21 one can see that in contrast to previous calculations [62], the necklace model for UHECR can explain only the highest energy part of the spectrum, with the AGASA excess somewhat above the prediction. This is the direct consequence of the new spectrum of particles in  $X$  decays obtained in this work. Thus UHE particles from necklaces can serve only as an additional component in the observed UHECR flux.

## 7 Conclusions

In this paper we have compared the MC and DGLAP methods for the calculation of hadron spectra produced by the decay (or annihilation) of superheavy  $X$  particles with masses up to  $M_{\text{GUT}} \sim 1 \times 10^{16} \text{ GeV}$ . We found an excellent agreement of these two methods.

We have further elaborated the MC simulation of Ref. [33], including the low-energy motivated hadronization functions  $f_i^h(x, Q_0)$  with the properties of fragmentation function  $D_i^h(x, Q_0)$  at low scale  $Q_0 \sim 1 \text{ GeV}$ . Though the new hadronization functions are somewhat different from the old ones, all new spectra computed for different initial partons  $i$  and different scales  $M_X$  agree very well with the old spectra, as it should be (see Section 3). The small differences in the spectra illustrate the uncertainties involved in the extraction of hadronization functions from experimental data. However, these uncertainties affect the spectra only at  $x > 0.2$ .

The calculations have been performed both for ordinary QCD and SUSY QCD. The inclusion of SUSY partons in the development of the cascade results only in small corrections, and it justifies our computation scheme with a single mass scale  $M_{\text{SUSY}}$ .

In comparison to the DGLAP method, the MC simulation has the advantage of including coherent branching. It allows reliable calculations at very small  $x$ . The Gaussian peak, the signature of the QCD spectrum, cannot be obtained using the DGLAP equations.

We have calculated the all-hadron spectra, as well as spectra of charged pions and nucleons, using the DGLAP equations. Two different methods (both based on our MC simulation) have been used.

In the first one we have used the initial fragmentation functions,  $D_q^h(x, M_Z)$  and  $D_g^h(x, M_Z)$ , the former determined from hadron spectrum measured from  $e^+e^-$ -annihilation at  $\sqrt{s} = M_Z$  and the latter calculated by MC. Then we evolved these fragmentation functions to higher scales  $M_X$  with the help of the DGLAP equations. In the second method we have used the hadronization functions as initial fragmentation functions, and evolved them from the scale  $Q_0 \sim 1 \text{ GeV}$  to  $M_X$ . In the first method the spectra calculated at different scales and for different initial partons are in excellent agreement between themselves and with MC at  $x \leq 0.3$  (see Figs. 11, 12).

In the second method the agreement is equally good at scales  $\sqrt{s} \gg M_Z$ . This also shows that hadronization functions can be seen as fragmentation functions at low scale  $Q_0 \sim 1 \text{ GeV}$ . At small scales the quark singlet FF is calculated less precisely.

The disagreement at  $x \sim 1$  is explained by the uncertainties in the calculations using DGLAP and MC at large  $x$ , especially in the latter. Using the hadronic fragmentation



functions we have calculated the spectra of photons (produced by decays of neutral pions), neutrinos (from charged pions) and nucleons.

Our nucleon spectrum agrees well with that of Refs. [43] and [44].

We compared also our spectrum of photons with the calculations of Ref. [43, 44, 34]. The comparison of the photon spectra is interesting, because of physical reasons (photons can be observable particles), and because the photon spectra are connected directly with the hadron spectra.

The spectra are in good agreement (see Section 5 for the detailed discussion). The disagreement at the largest  $x$  is not of great practical interest because of the model dependent prediction of the spectrum. Indeed, because of the non-perturbative character of the decay, many-parton decays of  $X$  particles can dominate over the two parton decay considered (see Section 4). Moreover, the range  $x > 0.3$  corresponds to too high energies  $E > 3 \times 10^{12}$  GeV at the masses of superheavy particles at interest  $M_X > 1 \times 10^{13}$  GeV.

We conclude that all calculations are in a good agreement especially at small  $x$  and the predicted shape of the generation spectrum ( $\propto dE/E^{1.9}$ ) can be considered as a signature of models with decaying (annihilating) superheavy particles.

The predicted spectrum of SHDM model cannot fit the observed UHECR spectrum at  $1 \times 10^{18}$  eV  $\leq E \leq (6 - 8) \times 10^{19}$  eV (see Fig 19). Only events at  $E \gtrsim (6 - 8) \times 10^{19}$  eV, and most notably the AGASA excess at these energies, can be explained in this model. The robust prediction of this model is photon dominance. In present calculations this excess diminishes to  $\gamma/N \simeq 2 - 3$  (see Fig. 18).

According to the recent calculation of Ref. [26], the muon content of photon induced EAS at  $E > 1 \times 10^{20}$  eV is high, but lower by a factor 5 – 10 than in hadronic showers. The muon content of EAS at  $E > 1 \times 10^{20}$  eV has been recently measured in AGASA [25]. The measured value is the muon density at the distance 1000 m from the shower core,  $\rho_\mu(1000)$ . From 11 events at  $E > 1 \times 10^{20}$  eV the muon density was measured in 6. In two of them with energies about  $1 \times 10^{20}$  eV,  $\rho_\mu$  is almost twice higher than predicted for gamma-induced EAS. Taking into account the contribution of extragalactic protons at this energy (see Ref. [70] for an analysis), the ratio  $\gamma/p$  predicted by the SHDM model is 1.2 – 1.4. It is lower than the upper limit  $\gamma/p \leq 2$  obtained by AGASA at  $E = 3 \times 10^{19}$  eV on the basis of a much larger statistics. The muon content of the remaining 4 EAS marginally agrees with that predicted for gamma-induced showers. The contribution of extragalactic protons for these events is negligible, and the fraction of protons in the total flux can be estimated as  $0.25 \leq p/\text{tot} \leq 0.33$ . This fraction gives a considerable contribution to the probability of observing 4 showers with slightly increased muon content. Not excluding the SHDM model, the AGASA events give no evidence in favor of it.

The simultaneous observation of UHECR events in fluorescent light and with water Cherenkov detectors has a great potential to distinguish between photon and proton induced EAS. An anisotropy towards the direction of the Galactic Center is another signature of the SHDM model. Both kinds of informations from Auger [71] will be crucial for the SHDM model and other top-down scenarios.

Topological defect models are another case when short-lived superheavy particle decays can produce UHECR. In Fig. 21 the spectra from necklaces are presented. One can see that at  $E \gtrsim 1 \times 10^{20}$  eV photons dominate, and the discussion in the previous paragraph applies here too. In contrast to previous calculations [62], the agreement with observations is worse: necklaces can explain only the highest energy part of the spectrum in Fig. 21, with the AGASA excess somewhat above the prediction. In the other energy ranges, UHE particles from necklaces can provide only a subdominant component. Other TDs suffer

even more problems (see Ref. [62]).

## Acknowledgments

We thank Pasquale Blasi for participation in the calculation of the spectra from necklaces. Cyrille Barbot and Ramon Toldrà are thanked for sending us their results and for helpful comments. Finally, we gratefully acknowledge useful discussions with Giuseppe Di Carlo, Motohiko Nagano, Sergey Ostapchenko, and in particular with Valery Khoze. MK is grateful to the Deutsche Forschungsgemeinschaft (DFG) for an Emmy Noether fellowship. This work has been performed within the INTAS project 99-01065.

## References

- [1] M. Takeda *et al.* [AGASA collaboration], astro-ph/0209422.
- [2] K. Greisen, Phys. Rev. Lett. **16**, 748 (1966); G.T. Zatsepin and V.A. Kuzmin, JETP Lett. **4**, 78 (1966) [Pisma Zh. Eksp. Teor. Fiz. **4**, 114 (1966)].
- [3] T. Abu-Zayyad *et al.* [HiRes collaboration], astro-ph/0208243.
- [4] e.g. V.S. Berezhinsky, A. Gazizov and S. Grigorieva, hep-ph/0204357; M. Kachelrieß, D. V. Semikoz and M. A. Tórtola, Phys. Rev. D **68**, 043005 (2003).
- [5] P.G. Tinyakov and I.I. Tkachev, JETP Lett., **74**, 445 (2001); astro-ph/0301336 (and references therein).
- [6] D.J. Bird *et al.* [Fly's Eye collaboration], Ap.J. **424**, 491 (1994).
- [7] N. Hayashida *et al.* [AGASA collaboration], Phys. Rev. Lett. **73**, 3491 (1994).
- [8] V.S. Berezhinsky, A. Gazizov and S. Grigorieva, hep-ph/0204357.
- [9] P. Sokolsky, Proc. of SPIE Conf. on Instrumentation for Particle Astrophysics, Hawaii (2002).
- [10] A.V. Glushkov *et al.* [Yakutsk collaboration], JETP Lett., **71**, 97 (2000).
- [11] V.S. Berezhinsky and S.I. Grigorieva, Astron. Astroph. **199**, 1 (1988); S. Yoshida and M. Teshima, Progr. Theoret. Phys., **89**, 883 (1993).
- [12] V.S. Berezhinsky, A. Gazizov and S. Grigorieva, astro-ph/0210095.
- [13] S.L. Dubovsky, P.G. Tinyakov and I.I. Tkachev, Phys. Rev. Lett. **85**, 1154 (2000); Z. Fodor and S.D. Katz, Phys. Rev. D **63**, 023002 (2000).
- [14] C. Isola and G. Sigl, Phys. Rev. D **66**, 083002 (2002).
- [15] H. Yoshiguchi, S. Nagataki, S. Tsurabi and K. Sato, astro-ph/0210132.
- [16] V.S. Berezhinsky and G.T. Zatsepin, Phys. Lett. **B28**, 423 (1969); Z. Fodor, S.D. Katz, A. Ringwald, and H. Tu, Phys. Lett. B **561**, 191 (2003), P. Jain, D.W. McKay, S. Panda and J.P. Ralston, Phys. Lett. **B484**, 267 (2000); but see also M. Kachelrieß and M. Plümacher, Phys. Rev. D **62**, 103006 (2000).
- [17] D.J.H. Chung, G.R. Farrar and E.W. Kolb, Phys. Rev. D **57**, 4606 (1998); V.S. Berezhinsky and M. Kachelrieß, Phys. Lett. **B422**, 163 (1998); I.F. Albuquerque, G.R. Farrar and E.W. Kolb, Phys. Rev. D **59**, 015021 (1999); V.S. Berezhinsky, M. Kachelrieß and S. Ostapchenko, Phys. Rev. D **65** 083004 (2002); M. Kachelrieß, D. V. Semikoz and M. A. Tórtola, Phys. Rev. D **68**, 043005 (2003).

- [18] D. Fargion, B. Mele and A. Salis, *Ap. J.* **517**, 725 (1999); T.J. Weiler, *Astrop. Phys.* **11**, 303 (1999); Z. Fodor, S.D. Katz and A. Ringwald, astro-ph/0203198.
- [19] D.A. Kirzhnits and V.A. Chechin, *Sov. J. Nucl. Phys.* **15**, 585 (1971); S. Coleman and S.L. Glashow, *Phys. Rev.* **D59**, 116008 (1999); R. Aloisio, P. Blasi, P.L. Ghia and A.F. Grillo, *Phys. Rev.* **D62**, 053010 (2000).
- [20] V.S. Berezinsky, *Nucl. Phys. (Proc. Suppl)* **B87**, 387 (2000).
- [21] V.A. Kuzmin and I.I. Tkachev, *Phys. Rep.* **320**, 199 (1999).
- [22] C.T. Hill, *Nucl. Phys.* **B224**, 469 (1983); P. Bhattacharjee and G. Sigl, *Phys. Rev.* **D51**, 4079 (1995).
- [23] V.S. Berezinsky and A. Vilenkin, *Phys. Rev. Lett.* **79**, 5202 (1997).
- [24] P. Blasi, R. Dick and E.W. Kolb, *Astrop. Phys.* **18**, 57 (2002).
- [25] K. Shinozaki *et al.* [AGASA collaboration], *Astrophys. J.* **571**, L 117 (2002).
- [26] A.V. Plyasheshnikov and F.A. Aharonian, *J. Phys.* **G28**, 267 (2002).
- [27] F.A. Aharonian, B.L. Kanevsky and V.A. Sahakian, *J. Phys.* **G17**, 1909 (1991).
- [28] J.N. Capdevielle, C. Le Gall and Kh.N. Sanosyan, *Astrop. Phys.* **13**, 259 (2000).
- [29] M. Birkel and S. Sarkar, *Astrop. Phys.* **9**, 297 (1998).
- [30] Yu.L. Dokshitzer and S.I. Troyan, Leningrad preprint, LNPI-922 (1984); Ya.I. Azimov, Yu.L. Dokshitzer, V.A. Khoze and S.I. Troyan, *Z. Phys.* **C27**, 65 (1985), *ibid.* **C31**, 213 (1986).
- [31] V.A. Khoze and W. Ochs, *Int. J. Mod. Phys.* **A12**, 29149 (1997).
- [32] V.S. Berezinsky and M. Kachelrieß, *Phys. Lett.* **B434**, 61 (1998).
- [33] V.S. Berezinsky and M. Kachelrieß, *Phys. Rev.* **D63**, 034007 (2001).
- [34] S. Sarkar and R. Toldrà, *Nucl. Phys.* **B621**, 495 (2002).
- [35] G. Marchesini and B.R. Webber, *Nucl. Phys. B* **238**, 1 (1984).
- [36] V.N. Gribov and L.N. Lipatov, *Sov. J. Nucl. Phys.* **15**, 438 (1972); L.N. Lipatov, *Sov. J. Nucl. Phys.* **20**, 94 (1975); Yu. L. Dokshitzer, *Sov. Phys. JETP* **46**, 641 (1977).
- [37] G. Altarelli and G. Parisi, *Nucl. Phys.* **B126**, 298 (1977).
- [38] N.A. Rubin, Thesis, Cavendish Laboratory, University of Cambridge (1999).
- [39] Z. Fodor and S. D. Katz, *Phys. Rev. Lett.* **86**, 3224 (2001).
- [40] C. Coriano, *Nucl. Phys.* **627**, 66 (2002).
- [41] C. Coriano and A. E. Faraggi, *Phys. Rev.* **D65**, 075001 (2002).
- [42] R. Toldra, *Comput. Phys. Commun.* **143**, 287 (2002).
- [43] C. Barbot and M. Drees, *Phys. Lett.* **B533**, 107 (2002).
- [44] C. Barbot and M. Drees, *Astropart. Phys.* **20**, 5 (2003).
- [45] A. Ibarra and R. Toldrà, *JHEP* **0206**, 006 (2002).
- [46] B. A. Kniehl, G. Krämer and B. Pötter, *Nucl. Phys.* **B 582**, 514 (2000).
- [47] V.S. Berezinsky, M. Kachelrieß and S. Ostapchenko, *Phys. Rev. Lett.* **89**, 171802 (2002).

- [48] C. Kounnas and D.A. Ross, Nucl. Phys. **B214**, 317 (1983); S.K. Jones and C.H. Llewellyn-Smith, Nucl. Phys. **B217**, 145 (1983).
- [49] G. Altarelli, Phys. Rept. **81**, 1 (1982).
- [50] J. Binnewies, B.A. Kniehl and G. Kramer, Phys. Rev. **D52**, 4947 (1995).
- [51] R. Itoh *et al.* [TOPAZ collaboration], Phys. Lett. **B345**, 335 (1995).
- [52] P. Abreu *et al.* [DELPHI collaboration], Z. Phys. **C73**, 11 (1996); G. Alexander *et al.* [OPAL collaboration], *ibid* **72**, 191 (1996).
- [53] D. Buskulic *et al.* [ALEPH collaboration], Z. Phys. **C66**, 355 (1995); D. Akers *et al.* [OPAL collaboration], Z. Phys. **C63** 181 (1994).
- [54] T. K. Gaisser *Cosmic rays and particle physics*, Cambridge University Press 1990.
- [55] V. Berezhinsky, M. Kachelrieß and A. Vilenkin, Phys. Rev. Lett. **79**, 4302 (1997)
- [56] V.A. Kuzmin and V.A. Rubakov, Phys. Atom. Nucl. **61**, 1028 (1998) [*Yad. Fiz.* **61** 1122 (1998)].
- [57] V.A. Kuzmin and I.I. Tkachev, JETP Lett. **68**, 271 (1998); D.J.H. Chung, E.W. Kolb and A. Riotto, Phys. Rev. **D59**, 023501 (1999).
- [58] D.N. Spergel *et al.* [WMAP collaboration], astro-ph/0302209.
- [59] P. Blasi and R.K. Sheth, Phys. Lett. **B486**, 233 (2000).
- [60] J. Ellis, J.L. Lopez and D.V. Nanopolous, Phys. Lett. **B247**, 257 (1990); K. Hamaguchi, Y. Nomura and T. Yanagida, Phys. Rev. **D58**, 103503 (1998); K. Benakli, J. Ellis and D.V. Nanopolous, Phys. Rev. **D59**, 047301 (1999); K. Hamaguchi, I.K. Izawa, Y. Nomura and Y. Yanagida, Phys. Rev. **D60**, 125009 (1999); Y. Uehara, JHEP **0112**, 034 (2001); C. Coriano, A.E. Faraggi and M. Plümacher, Nucl. Phys. **B614**, 233 (2001).
- [61] S.L. Dubovsky and P.G. Tinyakov, JETP Lett. **68**, 107 (1998).
- [62] V.S. Berezhinsky, P. Blasi and A. Vilenkin, Phys. Rev. **D58**, 103515 (1998).
- [63] A. Vilenkin and E.P.S. Shellard, *Cosmic Strings and Other Topological Defects*, Cambridge University Press, Cambridge 1994.
- [64] C.T. Hill, D.N. Schramm and T.P. Walker, Phys. Rev. **D36**, 1007 (1987).
- [65] J.J. Blanco-Pillado and K.D. Olum, Phys. Rev. **D60**, 083001 (1999).
- [66] P. Sreekumar *et al.*, Ap.J., **494**, 523, (1998).
- [67] V.S. Berezhinsky and A. Yu. Smirnov, Ap. Sp. Sci. **32**, 463, (1975),  
V.S. Berezhinsky, S.V. Bulanov, V.A. Dogiel, V.L. Ginzburg and V.S. Ptuskin, *Astrophysics of Cosmic Rays*, North-Holland, 1999.
- [68] A.W. Strong, I.V. Moskalenko and O. Reimer, astro-ph/0306345.
- [69] R. Aloisio, V.S. Berezhinsky and P. Blasi, in preparation.
- [70] V. Berezhinsky, A. Gazizov and S. Grigorieva, astro-ph/0302483.
- [71] J. Blümer *et al.* [Auger Collaboration], J. Phys. **G29** 867 (2003).

Table 1: Splitting functions for QCD and SUSY QCD from [48] ( $C_F = 4/3$  and  $N_C = 3$ )

quark	gluon
$P_{qq}^{(0)}(x) = C_F \left[ \frac{2}{1-x} - 1 - x \right]$	$P_{qg}^{(0)}(x) = \frac{1}{2} [x^2 + (1-x)^2]$
$P_{gq}^{(0)}(x) = C_F \left[ \frac{1+(1-x)^2}{x} \right]$	$P_{gg}^{(0)}(x) = 2N_C \left[ \frac{1}{1-x} + \frac{1}{x} + x(1-x) - 2 \right]$
$P_{\bar{q}q}^{(0)}(x) = C_F x$	$P_{\bar{q}g}^{(0)}(x) = \frac{1}{2} [2x(1-x)]$
$P_{\bar{g}q}^{(0)}(x) = C_F [1-x]$	$P_{\bar{g}g}^{(0)}(x) = 2N_C [x^2 + (1-x)^2]$
squark	gluino
$P_{q\tilde{q}}^{(0)}(x) = C_F$	$P_{q\tilde{g}}^{(0)}(x) = \frac{1}{2} [1-x]$
$P_{g\tilde{q}}^{(0)}(x) = C_F \left[ 2\frac{1-x}{x} \right]$	$P_{g\tilde{g}}^{(0)}(x) = N_C \left[ \frac{1+(1-x)^2}{x} \right]$
$P_{\bar{q}\tilde{q}}^{(0)}(x) = C_F \left[ 2\frac{x}{1-x} \right]$	$P_{\bar{q}\tilde{g}}^{(0)}(x) = \frac{1}{2} x$
$P_{\bar{g}\tilde{q}}^{(0)}(x) = C_F$	$P_{\bar{g}\tilde{g}}^{(0)}(x) = N_C \left[ \frac{1+x^2}{1-x} \right]$

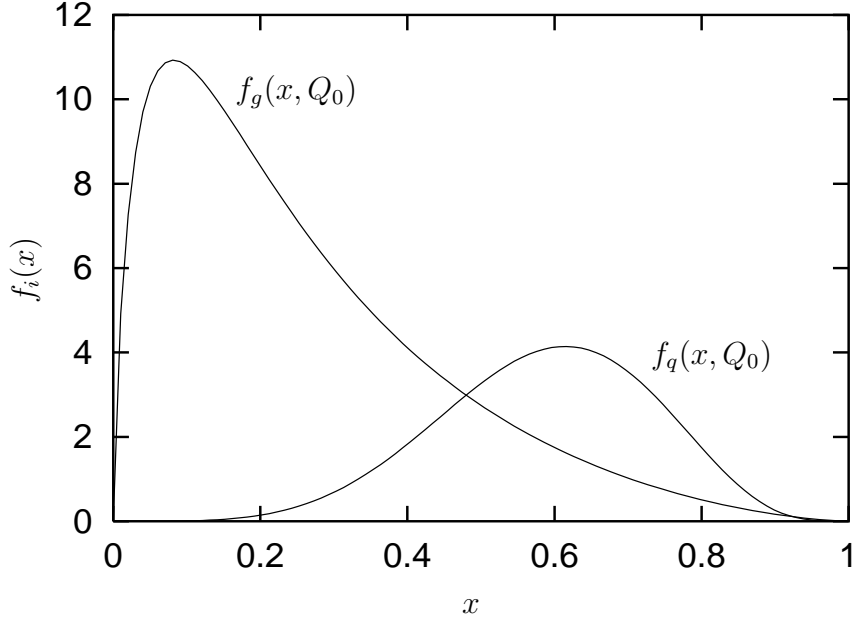


Figure 1: Hadronization functions for quarks  $f_q(x, Q_0)$  and gluons  $f_g(x, Q_0)$  obtained by fitting experimental data at  $\sqrt{s} = 91.2$  GeV and using  $Q_0^2 = 0.625$  GeV<sup>2</sup>.

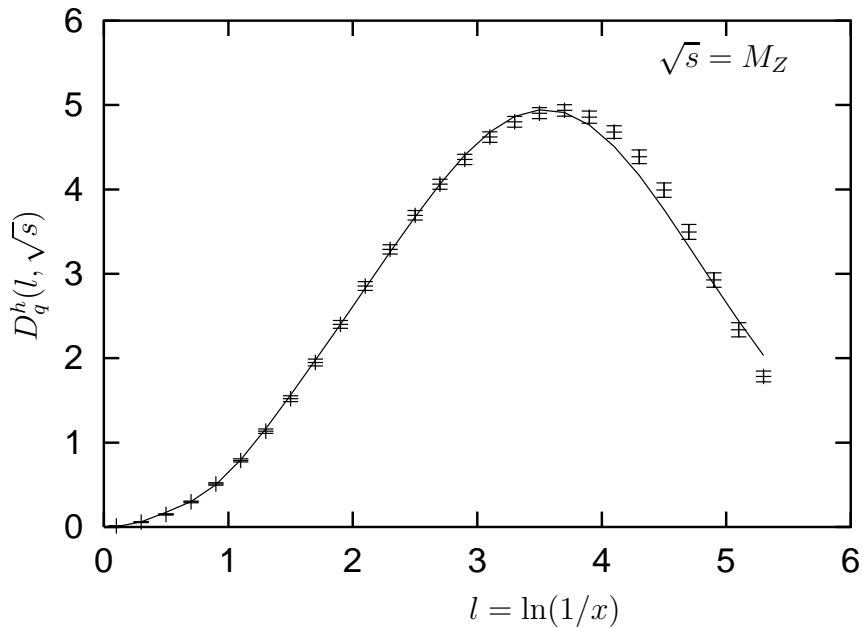


Figure 2: Comparison of the experimental data at  $\sqrt{s} = 91.2$  GeV and FF  $D_q^h(x, M_Z)$  computed by MC with hadronization functions as shown in Fig.1.

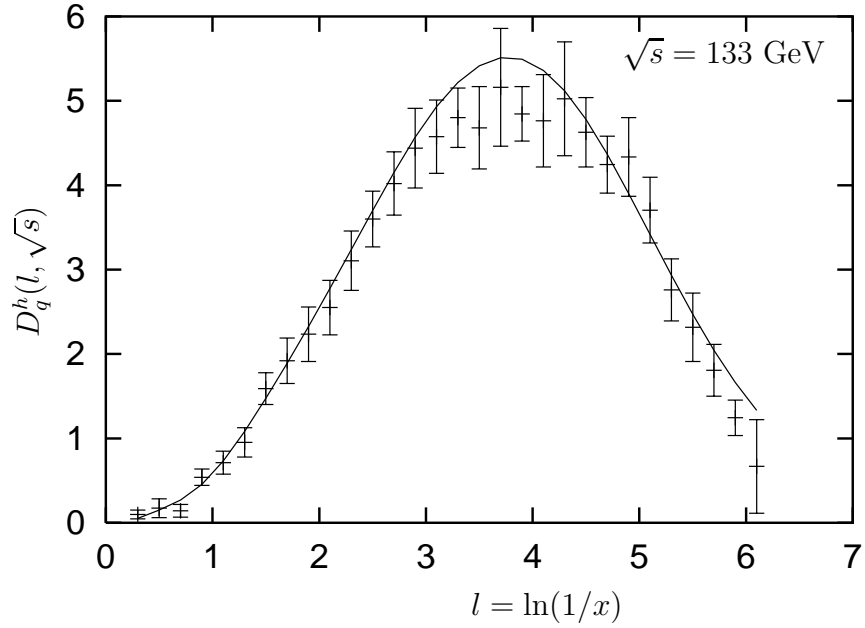


Figure 3: Comparison of MC computed FF  $D_q^h(x, \sqrt{s})$  with experimental data at  $\sqrt{s} = 133$  GeV.

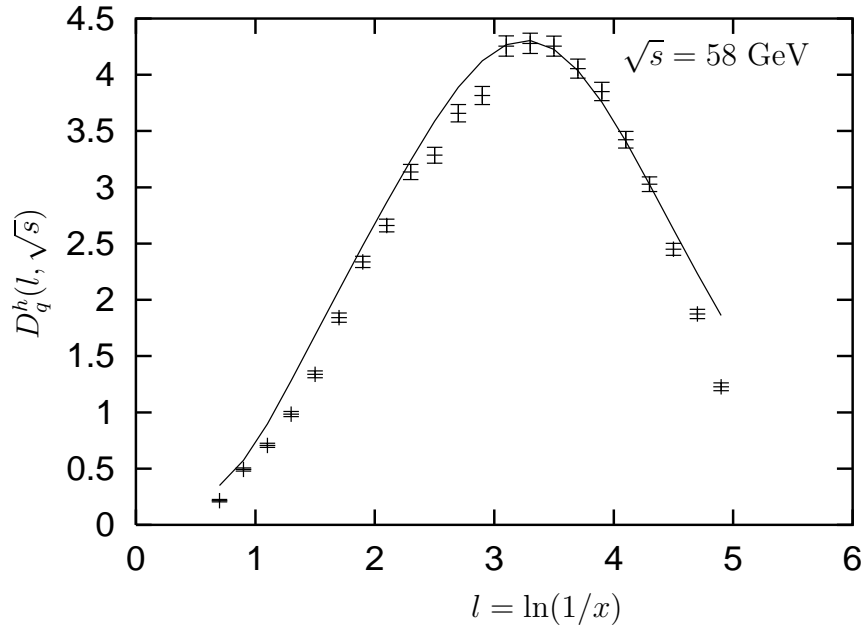


Figure 4: Comparison of MC computed FF  $D_q^h(x, \sqrt{s})$  with experimental data at  $\sqrt{s} = 58$  GeV.

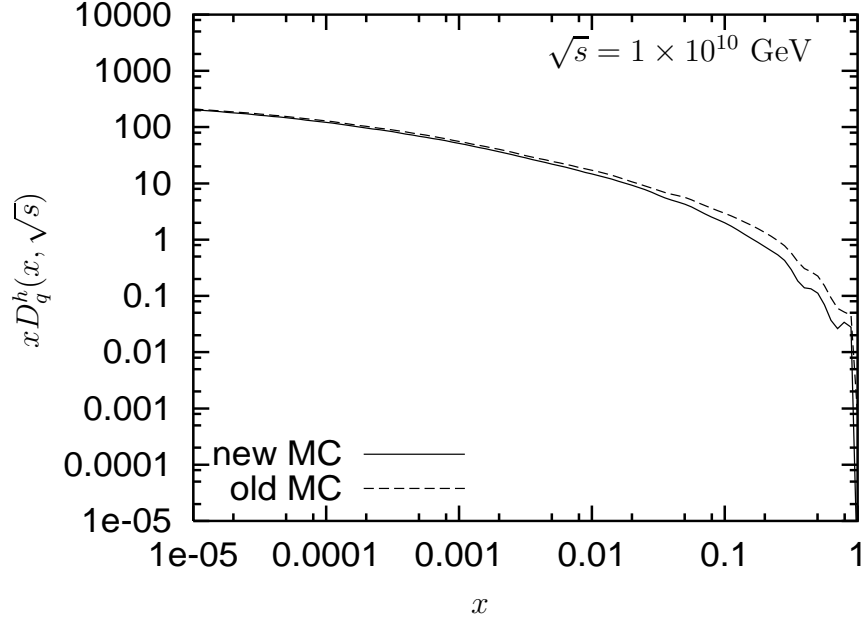


Figure 5: Comparison of spectra calculated with the old [33] and new hadronization functions: FFs from ordinary QCD MC with quark as a primary parton are displayed for the scale  $\sqrt{s} = 1 \times 10^{10}$  GeV for the new (solid line) and old (dashed line) hadronization functions.

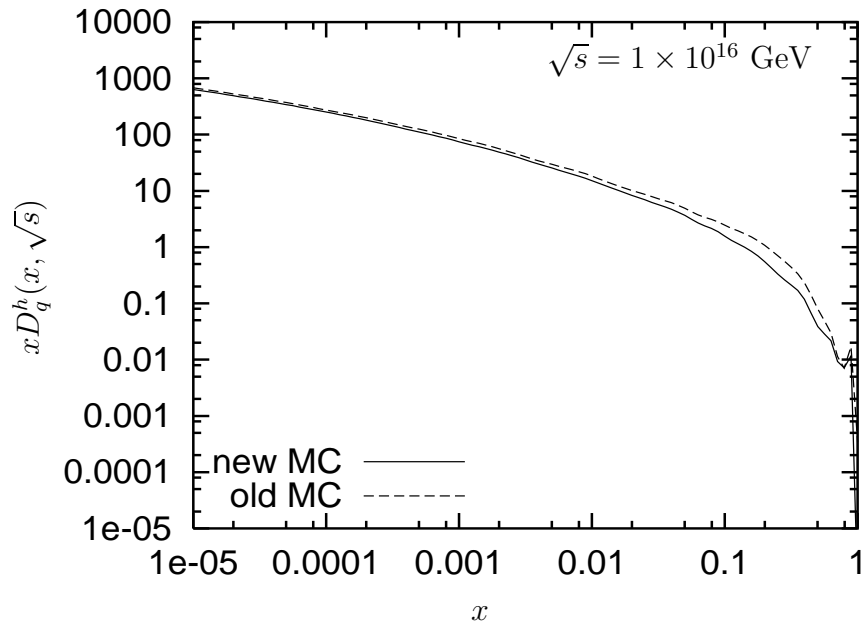


Figure 6: The same as in Fig. 5 for the scale  $\sqrt{s} = 1 \times 10^{16}$  GeV.



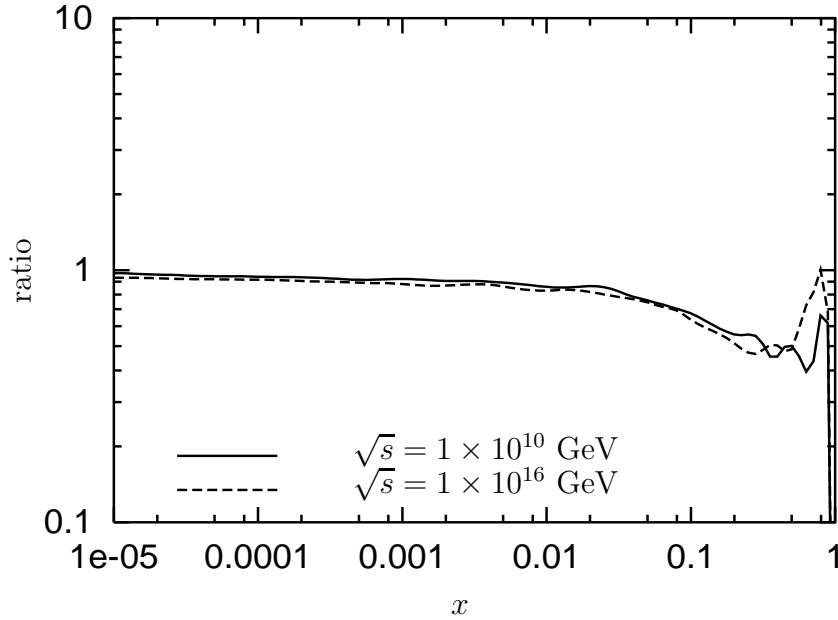


Figure 7: Ratio of the spectra calculated with the old and new hadronization functions for the scale  $\sqrt{s} = 1 \times 10^{10}$  GeV (solid line) and  $\sqrt{s} = 1 \times 10^{16}$  GeV (dashed line). For discussion of uncertainties at large  $x > 0.1$  see the text.

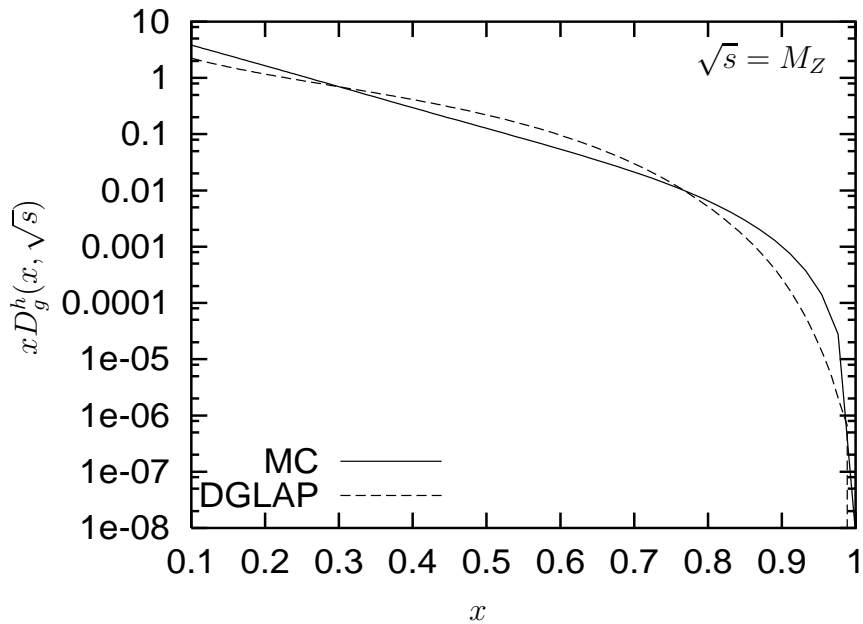


Figure 8: DGLAP FF with hadronization functions as initial fragmentation functions at the scale  $Q_0$ . The FF  $D_g^h(x, \sqrt{s})$  is DGLAP evolved from the scale  $\sqrt{s} = Q_0$  to the scale  $M_Z$  (dashed curve) and plotted in comparison with MC calculated  $D_g^h(x, M_Z)$  (full curve).

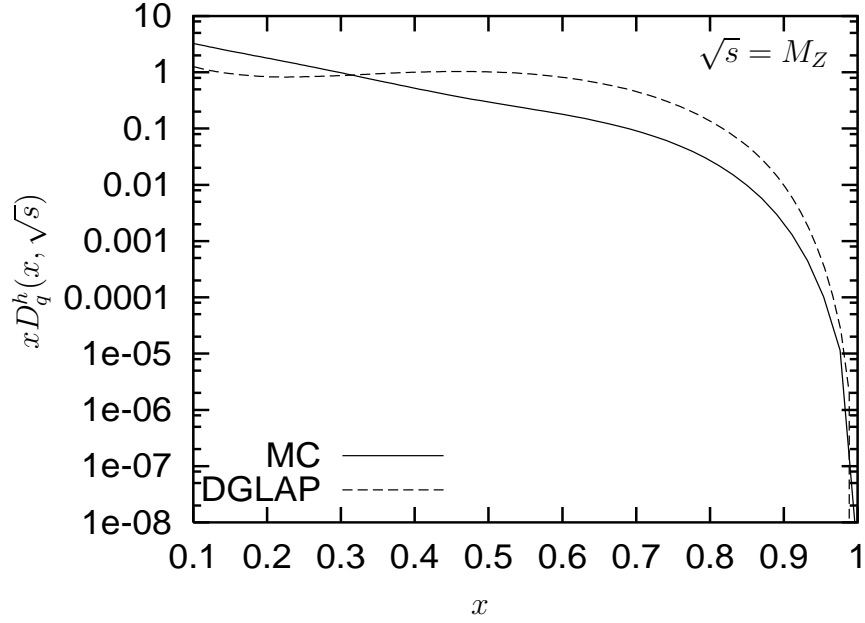


Figure 9: The same as in Fig. 8 for the quark FF  $D_q^h(x, M_Z)$ .

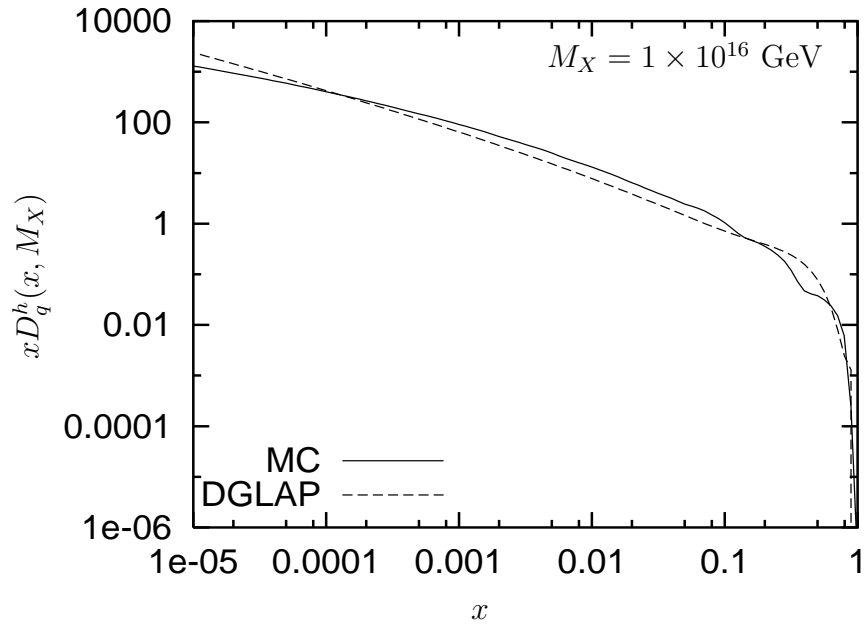


Figure 10: SUSY DGLAP FF with hadronization functions as initial fragmentation functions at the scale  $Q_0$ . The FF  $D_q^h(x, M_X)$  is SUSY DGLAP evolved from the scale  $\sqrt{s} = Q_0$  to scale  $M_X = 10^{16}$  GeV (dashed curve) and plotted in comparison with MC calculated  $D_q^h(x, M_Z)$  (full curve).

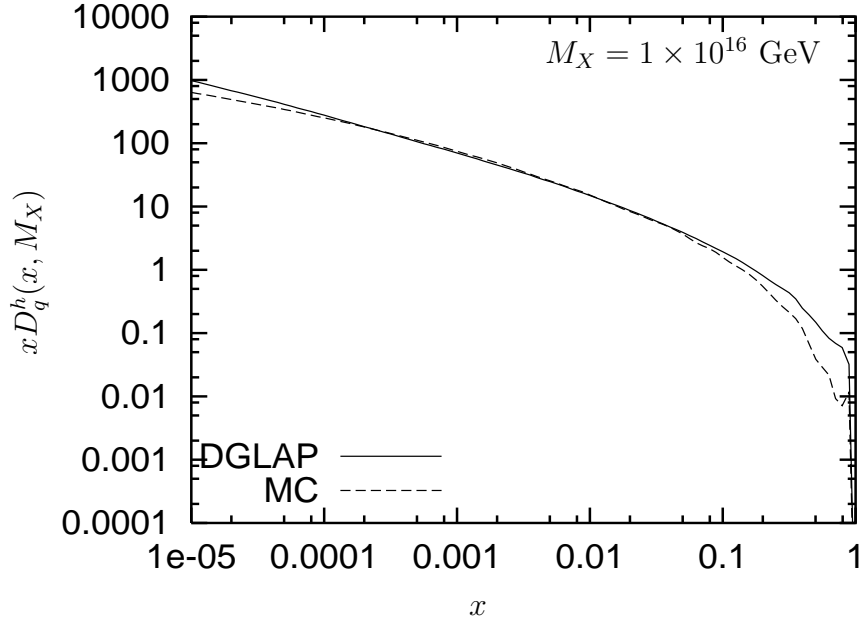


Figure 11: Comparison of the DGLAP FF (solid line) and MC FF (dashed line) for ordinary QCD with  $M_X = 1 \times 10^{16}$  GeV and with quark as a primary parton.

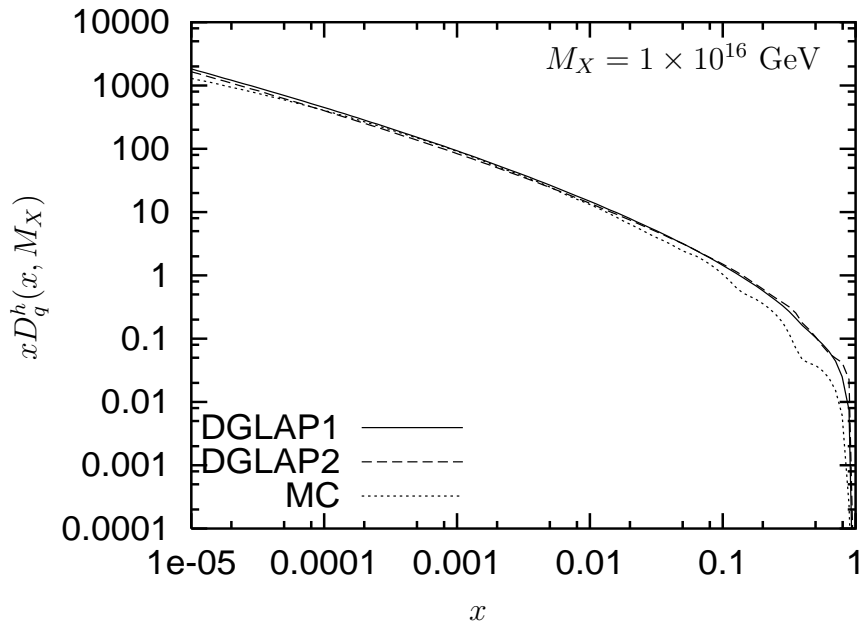


Figure 12: Comparison of SUSY DGLAP and SUSY MC fragmentation functions for  $M_X = 1 \times 10^{16}$  GeV with quark as a primary parton. SUSY DGLAP FFs are calculated for 10 TeV as the starting scale (solid line) and for  $M_Z$  (broken line). SUSY MC FF is shown by dotted line.

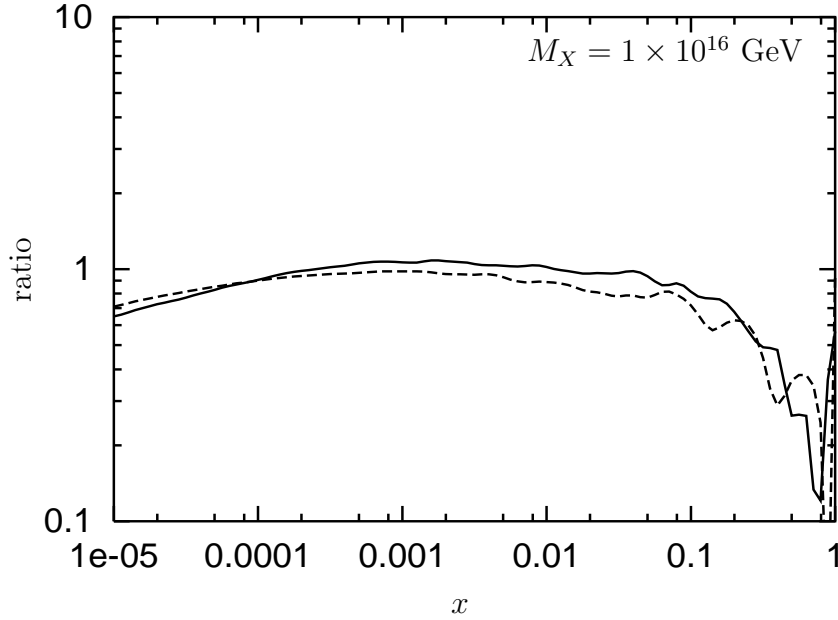


Figure 13: Ratio of FFs calculated by MC and DGLAP in ordinary QCD (solid curve) and SUSY QCD (dashed curve) for  $M_X = 1 \times 10^{16}$  GeV. For discussion see the text.

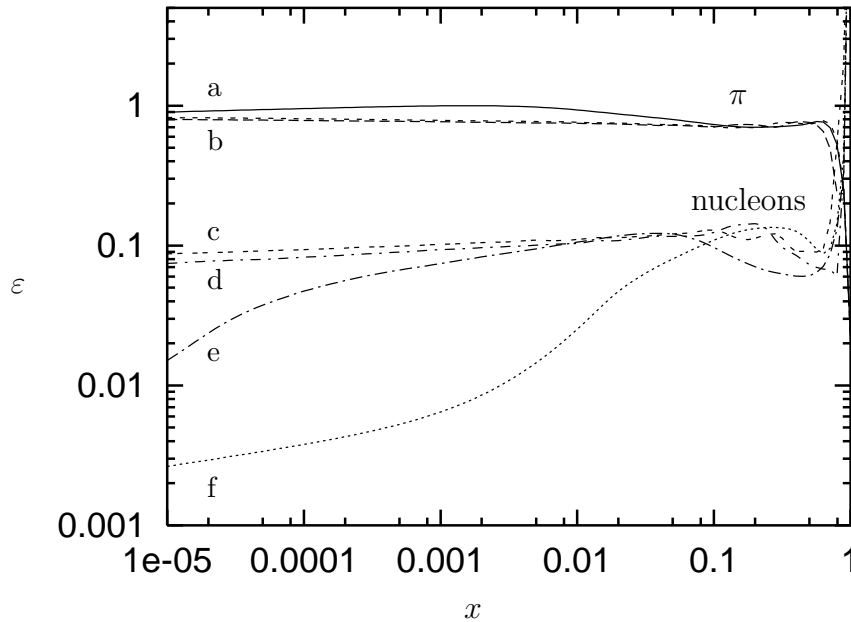


Figure 14: Fraction of pions,  $\epsilon_\pi$ , and nucleons,  $\epsilon_N$  relative to all hadrons according to SUSY MC simulations. For pions the curve *a* corresponds to  $M_X = M_Z$ , while curve *b* describes with a good accuracy the scales  $10^{10} \leq M_X \leq 10^{16}$  GeV. For nucleons curves *c*, *d*, *e*, *f* correspond to  $M_X$  equal to  $10^{16}$ ,  $10^{10}$ ,  $10^5$  GeV and  $M_Z$ , respectively.

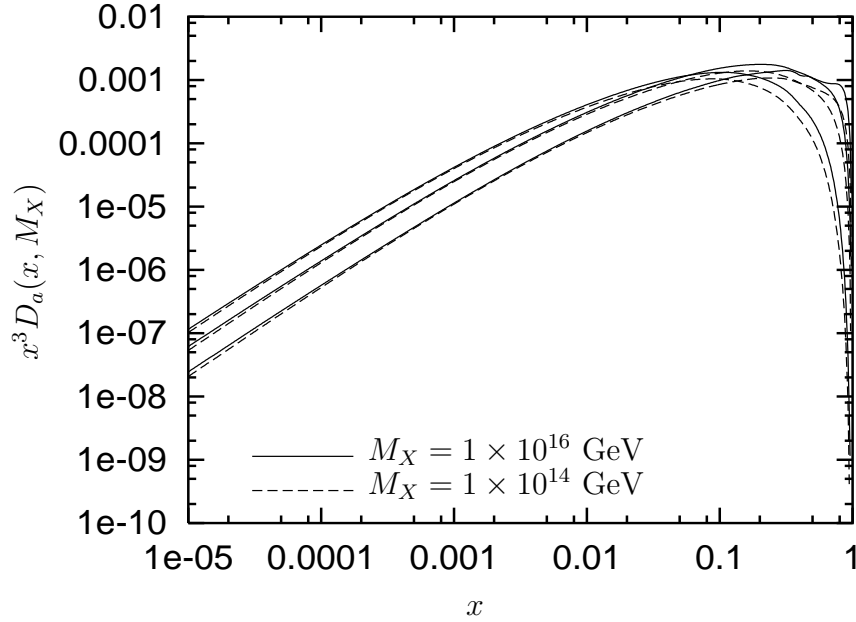


Figure 15: Neutrino (upper curves), gamma (middle curves) and nucleon (lower curves) spectra from DGLAP evolution at scales  $M_X = 1 \times 10^{16}$  GeV (solid line) and  $M_X = 1 \times 10^{14}$  GeV (dashed line). The spectra are obtained averaging over primary partons.

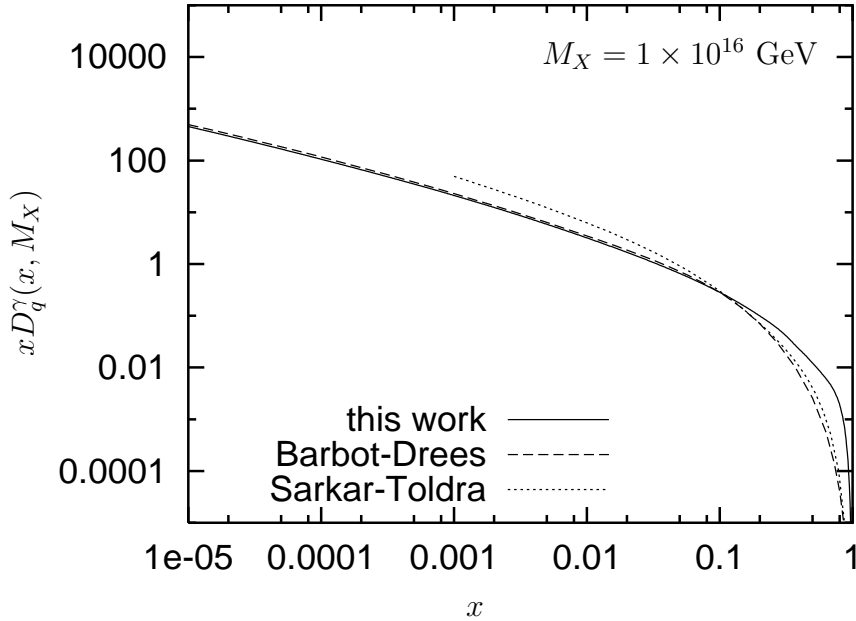


Figure 16: Comparison of photon spectra from present work computed with DGLAP equation (solid line), from [43, 44] (dashed line) and [34] (dotted line). All three calculations are performed with quark as initial parton for  $M_X = 1 \times 10^{16}$  GeV.

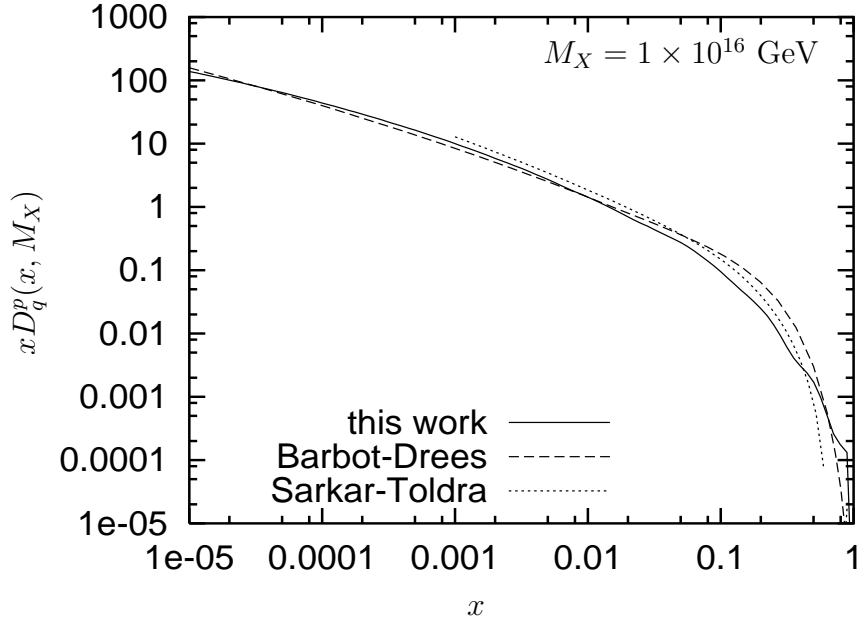


Figure 17: Comparison of proton spectra from present work computed with MC (solid line), from [43, 44] (dashed line) and from [34] (dotted line). All spectra are computed with quark as initial parton for  $M_X = 1 \times 10^{16}$  GeV.

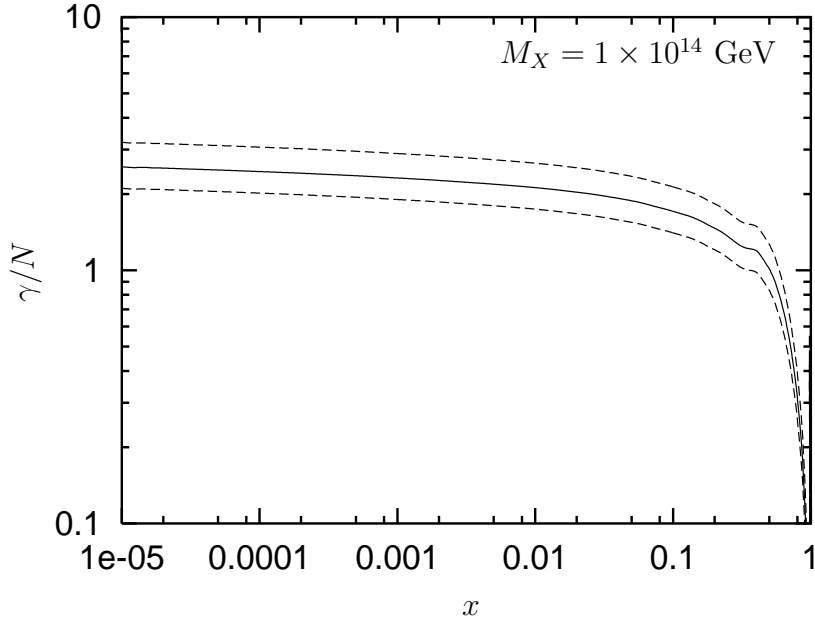


Figure 18: Gamma/nucleon ratio in generation spectra for  $M_X = 1 \times 10^{14}$  GeV computed with MC. The dashed curves illustrate the uncertainties of calculations. Calculations with DGLAP give very similar results.

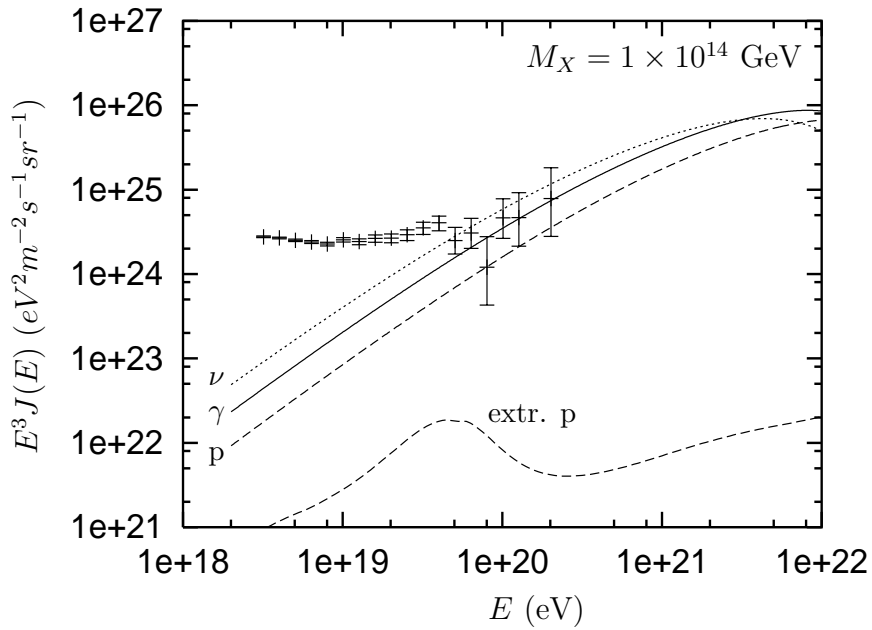


Figure 19: Spectra of neutrinos (upper curve), photons (middle curve) and protons (two lower curves) in SHDM model compared with AGASA data. The neutrino flux is dominated by the halo component with small admixture of extragalactic flux. The flux of extragalactic protons is shown by the lower curve.

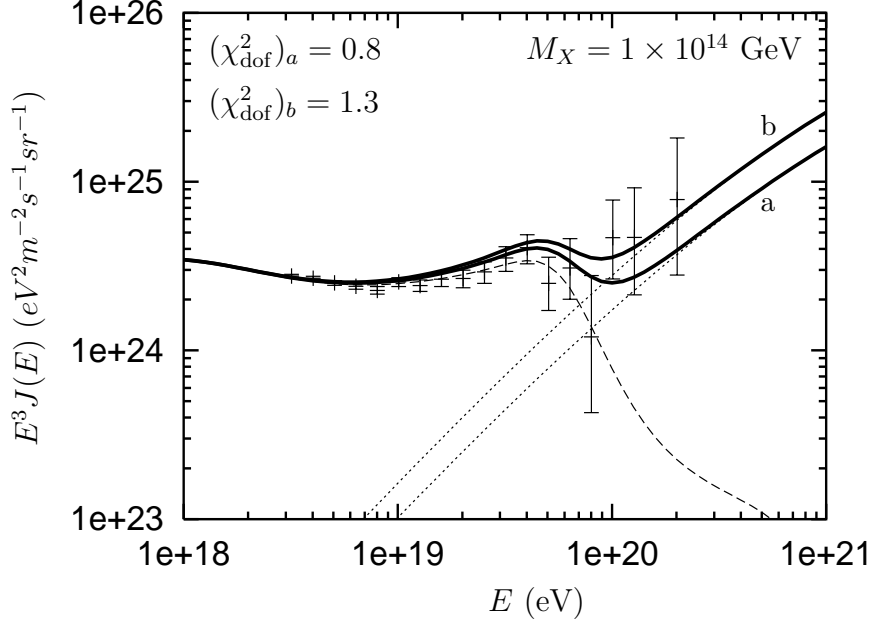


Figure 20: Comparison of SHDM prediction with the AGASA data. The calculated spectrum of SHDM photons is shown by dotted curves for two different normalizations. The dashed curve gives the spectrum of extragalactic protons in the non-evolutionary model of Ref. [70]. The sum of these two spectra is shown by the thick curves. The  $\chi^2$  values are given of the comparison of these curves with experimental data for  $E \geq 4 \times 10^{19}$  eV.

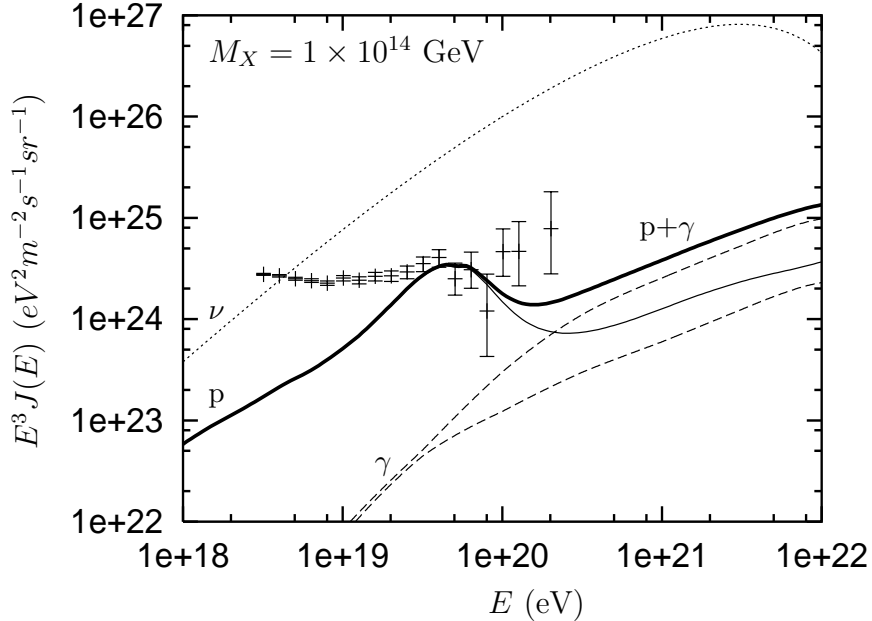


Figure 21: Diffuse spectra from necklaces. The upper curve shows neutrino flux, the middle - proton flux, and two lower curves - photon fluxes for two cases of absorption. The thick continuous curve gives the sum of the proton and higher photon flux.